International Journal of Environmental Research (2026) 20:131
https://doi.org/10.1007/s41742-026-01090-9

RESEARCH PAPER

Adsorption of Toxic Methylene Blue Dye from Aqueous Solutions Using *Thymbra spicata* L., Optimization by Taguchi Method and Investigation of Its Antioxidant Properties

Selenay Karadag[1] · Selen Avci Azkeskin[2] · Mesut Bilgi[1] · Birol Isik[1]

Received: 14 July 2025 / Revised: 23 September 2025 / Accepted: 30 March 2026
© The Author(s) 2026

Abstract

This study aimed to effectively evaluate various applications of *Thymbra spicata* L. biomass used in a zero-waste context. The study aimed to better understand the biomass's potential multifunctional uses in environmental remediation by evaluating its adsorption efficiency, methylene blue (MB) dye removal processes, and antioxidant properties. *T. spicata* L. biomass was characterized by Fourier transform infrared-attenuated total reflectance (FTIR-ATR), X-ray diffraction (XRD), scanning electron microscopy (SEM), and point of zero charge (pH_{pzc}). The optimum physicochemical parameters were optimized using the Taguchi method. The dye selectivity studies were conducted using various anionic and cationic dyes. Adsorption tests were carried out by adjusting the concentration (10–50 mg/L), period (0–120 min), pH (2–12), and dose (0.01–0.20 g/50 mL). We used equilibrium data to non-linear Langmuir, Freundlich, and Dubinin-Radushkevich (D-R) isotherm models. The results stated that the removal process occurred in a monolayer on the homogeneous surface of *T. spicata* L. biomass and the q_m value was determined as 65.03 mg/g at 298 K. Kinetic results showed that MB adsorption on *T. spicata* L. biomass followed a *pseudo-second order*. Thermodynamic tests showed that the process was exothermic ($\Delta H^o = -14.92\ kJ/mol$) and spontaneous ($\Delta G^o = -28.31\ kJ/mol$). In the second part, antioxidant capacity was determined by various methods using the extract of *T. spicata* L. biomass. The results of the study indicated that *T. spicata* L. could be a viable adsorbent for cationic dyes in aqueous solutions and a natural antioxidant source. Furthermore, compared to similar biomasses reported in the literature, it was found to be an alternative adsorbent.

✉ Birol Isik
isikb@yildiz.edu.tr

[1] Department of Chemistry, Faculty of Arts and Sciences, Yildiz Technical University, Esenler, Istanbul 34220, Turkey

[2] Department of Industrial Engineering, Kocaeli University, Izmit 41380, Turkey

Published online: 17 April 2026

Graphical Abstract

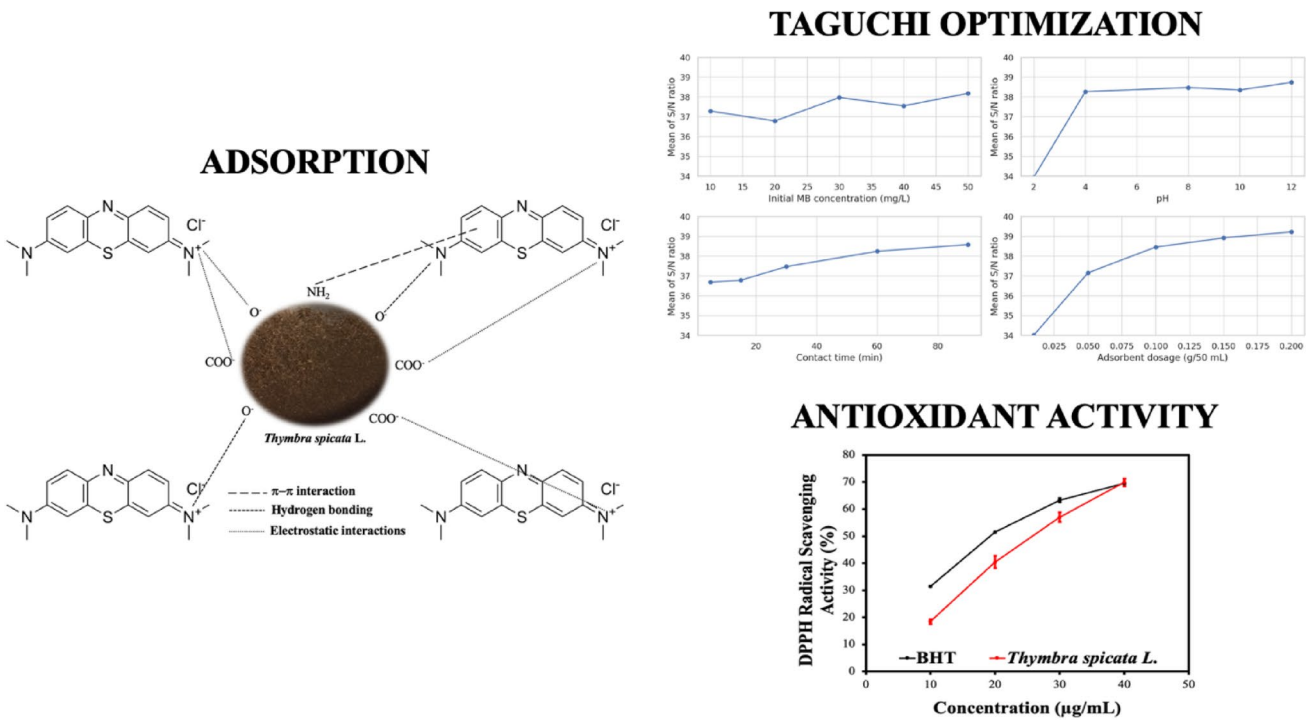

Highlights

- Methylene blue adsorption performance was determined as 92.70% at 298 K.
- The adsorption of methylene blue follows the *pseudo-second-order* kinetic model.
- The $q_m$values of *Thymbra spicata* L. reached up to 65.03 mg/g for methylene blue at 298 K
- The DPPH scavenging activity was determined as 69.89 ±1.36% at 40 µg/mL.

Keywords Adsorption · methylene blue · *Thymbra spicata* L. · Taguchi optimization · antioxidant capacity

Introduction

Water pollution has become a significant global concern, endangering human health and ecological systems. The issues have been greatly intensified by rapid industrialization, urbanization, and population increase (Assouani et al. 2024; El-Habacha et al. 2024; Moheb et al. 2025). Synthetic dyes have garnered significant attention among many contaminants due to their extensive application and enduring characteristics. Industries include textiles, leather, printing, cosmetics, and pharmaceuticals, which significantly contribute to dye-contaminated wastewater. These dyes frequently exhibit intricate chemical architectures, incorporating substituted chromophoric moieties such as azo, triarylmethane, and anthraquinone, rendering them significantly resistant to biodegradation. In anaerobic settings, certain chemicals may decompose, producing hazardous aromatic amines. Dye-laden effluents released into aquatic habitats can cause significant health problems, including carcinogenicity, mutagenicity, allergic dermatitis, skin irritation, and damage to essential organs such as the liver, kidneys, reproductive system, and central nervous system (Haydari et al. 2023; Bellaj et al. 2024; Xia et al. 2024; Zavala-Flores et al. 2024). Methylene blue (MB) [3, 7-bis (dimethyl amino) phenothiazine chloride tetra methylthionine chloride] is a synthetic dye utilized as a coloring agent for paper, wool, silk, and cotton. Due to extensive industrial applications, substantial quantities of effluent containing methylene blue dye are discharged into surface and groundwater. Toxic chemicals frequently accumulate in aquatic environments at concentrations reaching 1500 mg/L (Rafaqat et al. 2022; Alahmad et al. 2024). The distinctive stability of the aromatic ring in the MB molecular structure renders the chemical carcinogenic and non-biodegradable. The health risks associated with MB encompass genitourinary, respiratory, cardiovascular, central nervous system diseases, and dermatological

effects. Consequently, before the effluent contaminating the aquatic system, the dyes must be extracted to acceptable concentrations (Isik et al. 2023a; Ullah et al. 2024; Benhalima et al. 2024; Li et al. 2024; Braish et al. 2024; Shukla et al. 2024).

Effective and pragmatic strategies are crucial in tackling dye contamination issues. Diverse techniques have been explored for dye elimination, encompassing adsorption (Goswami et al. 2024), multi-stage coagulation and flocculation (Abou Taleb et al. 2025), ozonization (Jamali et al. 2024), sedimentation (Ma et al. 2025), filtration (Badawi et al. 2024), membrane technology (Hejji et al. 2024), chemical precipitation (Uddin et al. 2024), distillation (Omi et al. 2025), and reverse osmosis (Alkhouzaam and Khraisheh 2024). Among these approaches, adsorption is favored for its cost-effectiveness and efficiency, addressing the drawbacks of competing techniques, which include substantial investment costs, energy requirements, and the production of toxic waste. Activated carbons have emerged as the most extensively researched adsorbent utilized in water treatment systems for the removal of diverse chemical pollutants, including heavy metals and pigments. The global economy and population are expanding swiftly, resulting in a heightened demand for cost-effective, high-efficiency wastewater treatment technology (Chkirida et al. 2021; Soury et al. 2022; Lamberti et al. 2024; Aljeboree et al. 2025).

The adsorption process can be greatly impacted by several physicochemical factors, including pH, contact time, concentration, and amount of adsorbent. However, because there are too many experiments, optimizing process parameters and comprehending their association might be laborious and time-consuming. On the other hand, the design of experiments (DOE) method works better than conventional experimental techniques. By removing pointless sets of tests, the Taguchi design approach's usage of orthogonal arrays can broaden the procedure. Additionally, it offers comprehensive details on how the variables influencing the response variable interact. Additionally, DOE uses the response table to determine the optimal amount for each factor (Heidarinejad et al. 2020; Okolie et al. 2021; Patra et al. 2021).

In the adsorption process, a variety of materials are employed, including silica (Melnyk et al. 2021), activated carbon (Jawad et al. 2021), zeolite (Imessaoudene et al. 2023), montmorillonite (Al Kausor et al. 2022), biomass (Liu et al. 2022), polymers (Ali Khan et al. 2021), composites (Bellaj et al. 2024), and nanomaterials (Rasheed 2022). Research on biomass usage is being undertaken in numerous nations to mitigate the accumulation of biomass waste, particularly agricultural waste. The application of biomass is extensively employed for environmental sustainability by creating carbonaceous materials to eliminate diverse pollutants from wastewater and for energy generation, including hydrogen and ethanol. Identifying creative, cost-effective, and plentiful materials with exceptional adsorption characteristics is crucial, particularly given that the consumption of carbonaceous materials is rising by over 10% per year (Mbarki et al. 2019; Astuti et al. 2021, 2024).

In several parts of Türkiye, *Thymbra spicata* L. is cultivated as a medicinal and aromatic plant. *T. spicata* L. is a fragrant member of the mint family that can reach a height of 40 cm. It is used extensively in medicine as a tonic, respiratory tract disinfection, muscle and spasm reliever, parasite remover, and appetite enhancer. Additionally, it possesses antibacterial, antifungal, and antiparasitic qualities. The Lamiaceae family produces a variety of aromatic and terpenoid chemicals, which are then stored in the leaves, stems, epidermal glands, and reproductive tissue. The primary constituents of this plant's aerial portions include p-cymene, g-terpinene, carvacrol, and thymol (Kilic 2006; Matin et al. 2018; Erci et al. 2018). Considering plants contain a variety of natural molecules with different activities, including antioxidant activity, there is increasing attention to plants to obtain natural antioxidants instead of potentially harmful synthetic antioxidants like butylated hydroxytoluene (BHT) or butylated hydroxyanisole (BHA) (Peksel et al. 2010).

The aim and innovation of this study was to evaluate the performance of *T. spicata* L. as a biomass plant in various applications within the scope of zero waste. In this context, the biomass of *T. spicata* L. was used to remove toxic MB dye from wastewater, optimized using the Taguchi method, and the antioxidant properties of the biomass extract were evaluated. In this study, optimum adsorption conditions were determined and optimized using the Taguchi method. Adsorption studies were then conducted, and the raw data were applied to isotherm, kinetic, and thermodynamic equations. Furthermore, the antioxidant properties of the *T. spicata* L. biomass extract were determined using various methods.

Materials and Methods

Chemicals and Instrumentations

In experimental studies, methylene blue (MB) with the molecular formula $C_{16}H_{18}ClN_3S$ and ≥82% dye content, supplied by Sigma Aldrich, was used as a textile dye. *T. spicata* L. biomass was supplied by the local market and used as an adsorbent in adsorption studies. In addition, the extract of *T. spicata* L. biomass was used in antioxidant studies. Congo red (CR, $C_{32}H_{22}N_6Na_2O_6S_2$), Safranin O (SO, $C_{20}H_{19}N_4Cl$), Alizarin red S (ARS, $C_{14}H_7NaO_7S$), methyl orange (MO, $C_{14}H_{14}N_3NaO_3S$), crystal violet (CV, $C_{25}H_{30}N_3Cl$),

malachite green (MG, $C_{23}H_{25}N_2.C_2HO_4.0.5C_2H_2O_4$), and Rhodamine B (RhB, $C_{28}H_{31}ClN_2O_3$) textile dyes used during the dye selectivity study were supplied by Sigma Aldrich. 2,2-diphenyl-1-picrylhydrazyl (DPPH) and butylated hydroxytoluene (BHT) were supplied by Sigma Aldrich for use in antioxidant studies. 0.1 M NaOH and 0.1 M HCl solutions were used to adjust the solution pH during adsorption studies. Sodium nitrate ($NaNO_3$) used for pH_{pzc} studies was supplied by Sigma Aldrich. Sodium chloride (NaCl) and calcium chloride ($CaCl_2$), which were required to study the effect of different salt solutions on the adsorption process, were supplied by Sigma Aldrich.

The Nicolet IS10 Thermo FTIR-ATR device was used to obtain FTIR-ATR spectra both before and after adsorption to identify the functional groups in the structure during the evaluation of adsorbents. The morphology of biomass before and after adsorption was conducted by scanning electron microscopy (SEM, Zeiss EVO LS10). The adsorbent's crystal structure was ascertained using an XRD instrument of the PANalytical brand. Standard dye solutions and the supernatant portion following adsorption studies were analyzed using a Shimadzu UV2600 brand UV-vis spectrophotometer as a consequence of the adsorption experiments. The zeta potential analysis was conducted by Malvern Instruments Zetasizer.

Preparation of *T. spicata* L. Adsorbent

The *T. spicata* L. biomass, which was assessed as an adsorbent in the context of zero waste, was acquired for this study from the local market in Istanbul, Türkiye. To get rid of dirt, dust, and other contaminants on the biomass, it was carefully cleaned with distilled water. After being thoroughly cleaned, plants were dried for 24 h at 105 °C in a vacuum oven. Following the drying process, they were pulverized using a grinder and sieved to bring the particle size down to 80–100 mesh. Following the sieving procedure, they were dried for two hours at 60 °C and then placed in the sample container for use in adsorption research.

Preparation of *T. spicata* L. Extract

T. spicata L. biomass was ground and sieved through a 100 µm sieve. The obtained powder was used for the ultrasound-assisted extraction. For this, a 1:10 solid to solvent ratio was used, and ground *T. spicata* L. biomass was mixed with water. The mixture was sonicated in an ultrasonic bath for 5 min at 1-minute intervals. The resulting mixture was separated with a centrifuge at 6000 rpm for 5 min, and the solvent of the supernatant was evaporated. The obtained extract was used for further studies and kept at 4 °C.

Taguchi Experimental Design

As previously stated, process conditions can be effectively optimized with DOE while requiring the fewest possible experiments. Additionally, Taguchi-based DOE can be used to assess the interacting effects among process parameters. Additionally, DOE can be used to create an equation that shows how a set of process parameters and the response are related. An L25 orthogonal array was fitted with certain process levels and conditions to examine how various factors affected the response pattern. To reduce noise and design issues, Taguchi-based DOE considers the interior and external designs of the orthogonal arrays (Oladipo and Gazi 2015; Chowdhury et al. 2021; Yusuff et al. 2021). The usefulness of Taguchi design in analyzing the interplay of various factors and illustrating experimental responses is facilitated by its graphical portrayal. The Taguchi experimental design improves quality and stability while decreasing the impact of noise effects, which aids in assessing process performance. In every study, the quality losses for every attribute are measured using experimental values. Furthermore, the signal-to-noise ratio (S/N) is calculated from the value of the loss function. It can be defined as the ratio of the standard deviation to the mean value of the answer attributes. Optimal conditions can be obtained by combining the S/N ratio with analysis of variance (ANOVA). Additionally, the S/N ratio improves the average measurement by lowering variability. Higher-better, nominal-best, and lower-better quality qualities are the three categories utilized to examine the S/N ratio (Karmakar et al. 2018; Moralı et al. 2018; Okolie et al. 2021; Patra et al. 2021).

This optimization study aims to enhance the optimum physicochemical parameters for the process of adsorption. Four distinct steps make up the Taguchi design approach to process condition optimization. In the first phase, the response variable, that is, the ideal physicochemical characteristics, as well as the process parameters and their values, were specified. Second, based on the components and their levels, the Taguchi design type was chosen. Solution pH (2–12), adsorbent dosage (0.01–0.20 g/50 mL), initial concentration (10–50 mg/L), and contact time (0–120 min) were the parameters chosen for this investigation. The temperature was maintained at 298 K throughout all Taguchi experimental runs to isolate the effects of the chosen parameters and ensure consistency in the optimization process. Temperature was excluded as a variable in the Taguchi design of experiments (DOE). Nonetheless, it was assessed in the equilibrium tests performed under optimal conditions to measure the adsorption isotherms and thermodynamic characteristics. Minitab® Statistical Software 22.3.0 (Minitab, LLC, State College, USA) was used in the third phase to statistically model the experimental data. Verifying

the experimental results under ideal conditions by conducting a second set of trials under these circumstances was the last phase in the Taguchi design. The larger the S/N ratio, the better. For this purpose, the S/N ratio for the larger-is-better criterion can be calculated using Eq. (1).

$$\frac{S}{N} = -10\log\left[\frac{1}{n}\sum_{i=1}^{n}\frac{1}{y_i^2}\right] \quad (1)$$

Experimental parameters for MB removal from aqueous solution by *T. spicata* L. biomass were presented in Table 1.

Batch Adsorption Experiments

To investigate the effects of various physicochemical parameters on the adsorption process and to conduct equilibrium, kinetic, and thermodynamic studies, batch adsorption experiments were conducted in 50 mL dye solution in 100 mL conical flasks and in a heated and shaker water bath with a constant stirring speed of 120 rpm. 1000 mg/L of MB dye was added to a stock solution. The stock solution was prepared by evenly dissolving one gram of powdered pigment in 1,000 milliliters of distilled water. To prepare MB dye solutions for use in adsorption investigations, this stock solution was diluted with distilled water. The initial concentrations of these dye solutions were 10, 20, 30, 40, and 50 mg/L. Adsorption kinetic studies were conducted with constant amounts of adsorbent, initial concentrations, and pH values until the system reached equilibrium. Then, it was established that 0–120 min was the ideal kinetic working range for adsorption investigations. Initial concentrations between 10 and 50 mg/L, temperatures between 298 and 318 K, consistent pH values, constant contact times, and constant amounts of adsorbent were all used in the adsorption equilibrium investigations. The solutions were centrifuged for five minutes at about 9000 rpm following the conclusion of the adsorption tests. In a UV-vis spectrophotometer, the standard dye solutions and the supernatant solution that was left over after centrifugation were analyzed at a wavelength of 663 nm. Equations (2), (3), and (4) were used to obtain the adsorption percentage (R%), adsorption capacity at equilibrium (q_e, mg/g), and adsorption capacity following "t" time (q_t, mg/g) (Mobarak et al. 2018, 2019; Choudhary et al. 2020; Isik et al. 2024).

$$R\% = \frac{(C_o - C_e)}{C_o} \times 100 \quad (2)$$

$$q_e = (C_o - C_e) \times (V/m) \quad (3)$$

$$q_t = (C_o - C_t) \times (V/m) \quad (4)$$

In these equations, C_o, C_e, and C_t represent the initial, equilibrium and "t" time concentrations (mg/L), respectively. V represents the volume of the dye solution (0.05 L) and m represents the amount of adsorbent (g).

Dye selectivity tests and an investigation into the adsorption behavior of several cationic and anionic dyes on *T. spicata* L. biomass were conducted. In the experimental tests, the cationic dyes MB, SO, MG, RhB, and CV, as well as the anionic dyes MO, CR, and ARS, were employed for this purpose. 0.05 g of *T. spicata* L. biomass was added to 50 mL of water solutions containing different organic dyes at 20 mg/L dye concentrations to investigate the preferential adsorption of these dyes on *T. spicata* L. biomass. The dye selectivity experiments were conducted at a constant temperature of 298 K, and the pH was maintained at approximately 7, which is close to neutral and relevant for practical wastewater conditions. In a hot water bath using a shaker, the mixtures were agitated for 45 min at a speed of 120 rpm. At wavelengths of 663 nm, 519 nm, 615 nm, 554 nm, 591 nm, 465 nm, 498 nm, and 445 nm for MB, SO, MG, RhB, CV, MO, CR, and ARS dyes, respectively, the samples extracted from the solution medium were centrifuged for analysis in a UV-vis spectrophotometer following the adsorption process. The R% values of these dyes were calculated using Eq. (2).

Adsorption Isotherms, Kinetics, and Thermodynamics

Three separate adsorption isotherms—Langmuir (Langmuir 1918), Freundlich (Freundlich 1906), and Dubinin-Radushkevich (D-R) (Chu et al. 2024) were used to assess the relationship between the quantities of dye adsorbed on *T. spicata* L. biomass and the equilibrium concentration of MB dye in the aqueous phase. Equations (5), (6), and (7), respectively, provide the three isotherm models in non-linear forms (Isik 2023; Sismanoglu et al. 2025).

Table 1 Studied process parameters and their levels

Symbol	Parameter	Level				
		1	2	3	4	5
C	Initial MB concentration (mg/L)	10	20	30	40	50
p	pH	2	4	8	10	12
d	Adsorbent dosage (g/50 mL)	0.01	0.05	0.10	0.15	0.20
T	Contact time (min)	5	15	30	60	90

$$q_e = \frac{q_m \times K_L \times C_e}{1 + K_L \times C_e} \quad (5)$$

$$q_e = K_F \times C_e^{(1/n)} \quad (6)$$

$$q_e = q_{D-R} \times e^{-\beta \times \left(R \times T \times ln\left(1+\frac{1}{C_e}\right)\right)^2};\ E_{D-R} = (2\beta)^{-0.5} \quad (7)$$

In these equations, q_e represents the adsorption capacity at equilibrium (mg/g), q_m represents the maximum adsorption capacity calculated from the Langmuir isotherm (mg/g), K_L represents the Langmuir isotherm constant (L/mg), n and K_F represent the Freundlich isotherm constants, R represents the ideal gas constant (8.314 J/mol.K), q_{D-R} represents the theoretical adsorption capacity calculated from the D-R isotherm (mg/g), E_{D-R} represents the adsorption energy (kJ/mol).

To investigate the rate at which MB dye molecules were adsorbed by *T. spicata* L. biomass and to ascertain the adsorption mechanism, this work employed two non-linear kinetic models: *pseudo-first order* (Eq. 8) and *pseudo-second order* (Eq. 9) (Berkane et al. 2020; Isik et al. 2023b).

$$q_t = q_e \times \left(1 - e^{-k_1 \times t}\right) \quad (8)$$

$$q_t = \frac{q_e^2 \times k_2 \times t}{1 + q_e \times k_2 \times t} \quad (9)$$

In these equations, q_t represent the adsorption capacity at "t" time (mg/g); k_1 represent the *pseudo-first order* rate constant (min^{-1}); and k_2 represent the *pseudo-second order* rate constant (g/mg.min).

The impact of temperature was applied to the experimental data collected at 298, 308, and 318 K, respectively, to ascertain the thermodynamic parameters, comprehend the solid-liquid interface process, and investigate the nature of the adsorption process. The thermodynamic parameters were determined using the following formulas (Lima et al. 2019; Isik 2025).

$$K_e^o = \frac{1000 \times K_L \times M_{MB} \times [Adsorbate]^o}{\gamma} \quad (10)$$

$$\ln K_e^o = -\frac{\Delta G^o}{R \times T} = \frac{\Delta S^o}{R} - \frac{\Delta H^o}{R} \times \frac{1}{T} \quad (11)$$

$$\Delta G^o = \Delta H^o - T \times \Delta S^o \quad (12)$$

In these equations, K_e^o represents the thermodynamic equilibrium constant, M_{MB} represents the molecular weight of MB dye (319.8 g/mol), $[Adsorbate]^o$ represents the standard concentration of adsorbate (1 mol/L), γ represents the dimensionless factor, ΔG^o represents the Gibbs free energy (kJ/mol), ΔS^o represents the entropy of adsorption (J/mol.K), and ΔH^o represents the adsorption enthalpy (kJ/mol).

Error Functions

Non-linear regression or error analysis were used to examine isotherm and kinetic models using experimentally acquired data. The study data were analyzed and adjusted to fit models using the non-linear least squares method implemented in Microsoft Excel software. The quality of fit was assessed using statistical measures such as ARE (Absolute Relative Error), RMSE (Root Mean Square Error), SD (Standard Deviation), χ2 (Chi-Square), and SSE (Sum of Square Errors). These metrics were regarded as the primary evaluation standards. The statistical parameters and mathematical equations were shown as follows (Elkatory et al. 2024; Akgul et al. 2024):

$$SSE = \sum_{i=1}^{n} (q_{e,exp} - q_{e,cal})^2 \quad (13)$$

$$ARE = \frac{100}{n} \sum_{i=1}^{n} \left| \frac{q_{e,exp} - q_{e,cal}}{q_{e,exp}} \right| \quad (14)$$

$$RMSE = \sqrt{\frac{1}{n-2} \sum_{i=1}^{n} (q_{e,exp} - q_{e,cal})^2} \quad (15)$$

$$SD = \sqrt{\frac{1}{n} \sum_{i=1}^{n} (q_{e,cal} - q_{e,exp})^2} \quad (16)$$

$$\chi^2 = \sum_{i=1}^{n} \frac{(q_{e,exp} - q_{e,cal})^2}{q_{e,cal}} \quad (17)$$

In these equations, the estimated and experimental adsorption capacities in mg/g were denoted by the variables $q_{e,cal}$ and $q_{e,exp}$, respectively.

Total Phenolic Content

The extract's total phenolic content was determined with Folin-Ciocalteau reagent, and the method of Singleton et al. was used (Singleton et al. 1999). 0.1 mL extract at 1 mg/mL concentration was mixed with 4.5 mL distilled water, and 0.1 mL Folin-Ciocalteau reagent was added to the mixture. After mixing thoroughly, 3 min incubation was done. Then 0.3 mL 2% sodium carbonate solution was added and mixed. The mixture was incubated for 120 min at room temperature in the dark. At the end of the incubation, the absorbance of the samples was read at 760 nm. The same method was used for pyrocatechol to obtain a standard curve, and results were given as pyrocatechol equivalents per mg extract.

DPPH Radical Scavenging Activity

To evaluate the extract's ability to scavenge radicals, the DPPH method by Brand-Williams et al. was used (Brand-Williams et al. 1995). Briefly, a 20 mg/L DPPH solution was prepared. To 1.5 mL of this solution, 0.75 mL of the extract solution was added and mixed thoroughly. The mixture was incubated at room temperature in the dark for 30 min. The absorbance measurements were done at 517 nm. The extract solution was prepared at 10–40 µg/mL and compared with a standard antioxidant (BHT) at the same concentration. The radical scavenging activity of the extract was calculated with Eq. (18) where A_o shows the absorbance of the control solution and A_1 shows the absorbance of the sample.

$$Radical\ scavenging\ activity\ (\%) = ((A_o - A_1)/A_o) \times 100 \quad (18)$$

Total Antioxidant Capacity

The Prieto et al. method was applied to determine the extracts' total antioxidant capacity (Prieto et al. 1999). A reagent solution was made by mixing 30 mM sodium phosphate, 4 mM ammonium molybdate, and 600 mM sulfuric acid. 1 mL of this reagent was mixed with 0.1 mL of extract solution, and the mixture was then incubated at 95 °C for 90 min. Following the conclusion of the incubation period and the samples' cooling to room temperature, the absorbance was measured at 695 nm. Ascorbic acid was used to create the calibration curve, with concentrations ranging from 25 to 100 µg/mL. The results were presented as µg ascorbic acid/mg extract.

β-Carotene Bleaching Assay

This assay was done according to the method by Bruni et al. (Bruni et al. 2004). After dissolving 10 mg of trans-β-carotene in 10 mL of chloroform, 0.2 mL of the solution was added to 20 mg of linoleic acid and 200 mg of Tween-20. Following the chloroform's evaporation, 50 mL of distilled water was added and mixed. 5 mL of this solution was transferred to tubes with 0.2 mL (1 mg/mL) of the sample. The tubes were incubated in a water bath at 50 °C for 2 h. The solutions' absorbances at 470 nm were measured after 1 and 2 h. BHT was utilized as the standard. The bleaching activity of the extract was calculated compared to BHT.

Results and Discussion

Characterization of *Thymbra spicata* L. Biomass

FTIR-ATR spectra of the sample before and after adsorption were shown in Fig. 1. From the spectrum of the sample before adsorption, the peaks obtained at 3286, 1607, 1416, 1317, 1242, and 1018 cm^{-1} were related to the -OH stretching, C=O stretching, N–H (amide-II) in-plane bending vibration, S=O stretching, C-O stretching, and PO_4^{3-} stretching, respectively (Han et al. 2011; Boyatzis et al.

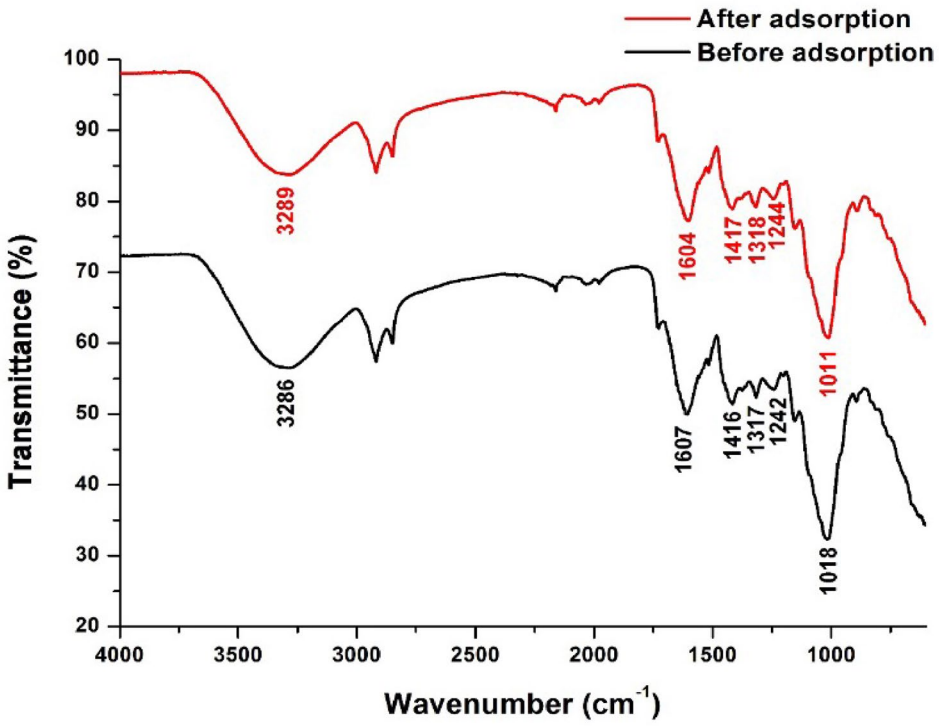

Fig. 1 The FTIR-ATR spectrum of *T. spicata* L. before and after MB dye adsorption

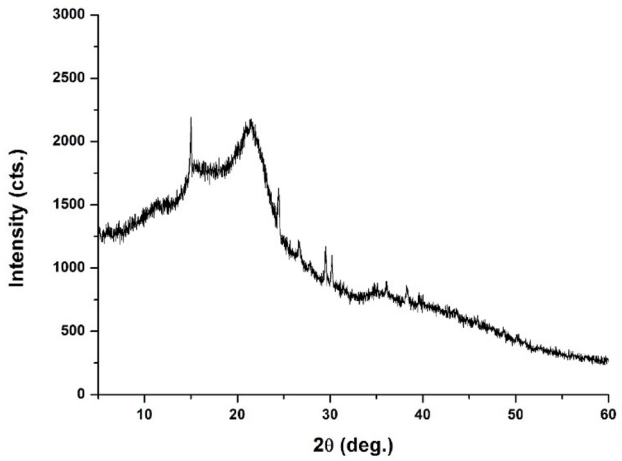

Fig. 2 The XRD pattern of *T. spicata* L. biomass

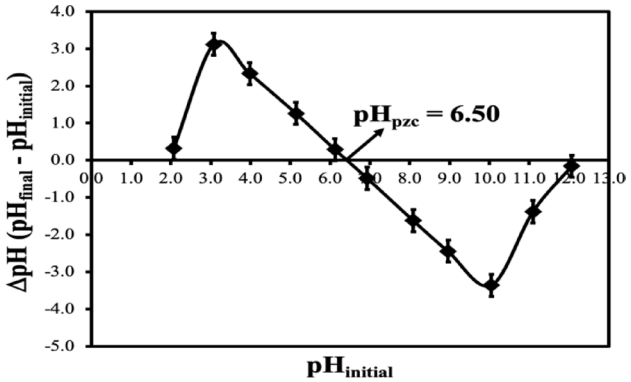

Fig. 4 The pH_{pzc} graph of *T. spicata* L. biomass

2016; Li et al. 2019a; Ding et al. 2020; Nguyen et al. 2021). The spectrum for the after-adsorption sample was almost like that before adsorption. However, after adsorption, the peaks mentioned above shifted, with new peaks appearing at 3289, 1604, 1417, 1318, 1244, and 1011 cm^{-1}, respectively. This indicated that electrostatic interactions occurred between the surface functional groups and the dye molecules, and the adsorption process was effective.

XRD spectrum of the sample was illustrated in Fig. 2. A spectrum corresponding to a high cellulose content with a broad peak at $2\theta = 21.4°$ was obtained. The range between $2\theta = 15°$ and $2\theta = 25°$ corresponds to the amorphous phases of lignin, hemicellulose, and cellulose (Isik 2025).

Figure 3 displayed the SEM images of *T. spicata* L. biomass. Before dye removal, *T. spicata* L. biomass was discovered to have a complicated, cleft, rough, and uneven surface that was appropriate for retaining MB dye. It was discovered that the surface of *T. spicata* L. biomass became nearly smooth and more uniform after the MB dye was removed from the water, and the dye also covered the surface irregularities.

To determine the *T. spicata* L. biomass's zero charge point (pH_{pzc}), experiments were conducted using the salt addition method (Dbik et al. 2020; Rose et al. 2023). 0.2 g of *T. spicata* L. biomass was added to 50 mL (0.1 M) of sodium nitrate solution that had been made in the initial pH ($pH_{initial}$) range of 2 to 12. To find the final pH (pH_{final}) values, solutions made at various pH levels were stored in a shaker at 25 °C for 48 h. A graph between $pH_{initial}$ and ΔpH ($pH_{final} - pH_{initial}$) data was used to calculate the pH_{pzc} value for the *T. spicata* L. biomass. Finding the pH_{pzc} value of the *T. spicata* L. plant is crucial for figuring out the pH at which the surface is electrostatically charge neutral. Figure 4 illustrates that the point of pH_{pzc} for *T. spicata* L. biomass is 6.50. This value is essential for comprehending the surface charge characteristics of the biomass across varying pH settings. At pH levels below the pH_{pzc}, the biomass surface exhibits a positive charge, enhancing the adsorption of anionic dye species. Conversely, at pH levels exceeding the pH_{pzc}, the surface acquires a negative charge, facilitating the adsorption of cationic dyes like methylene blue (MB). MB

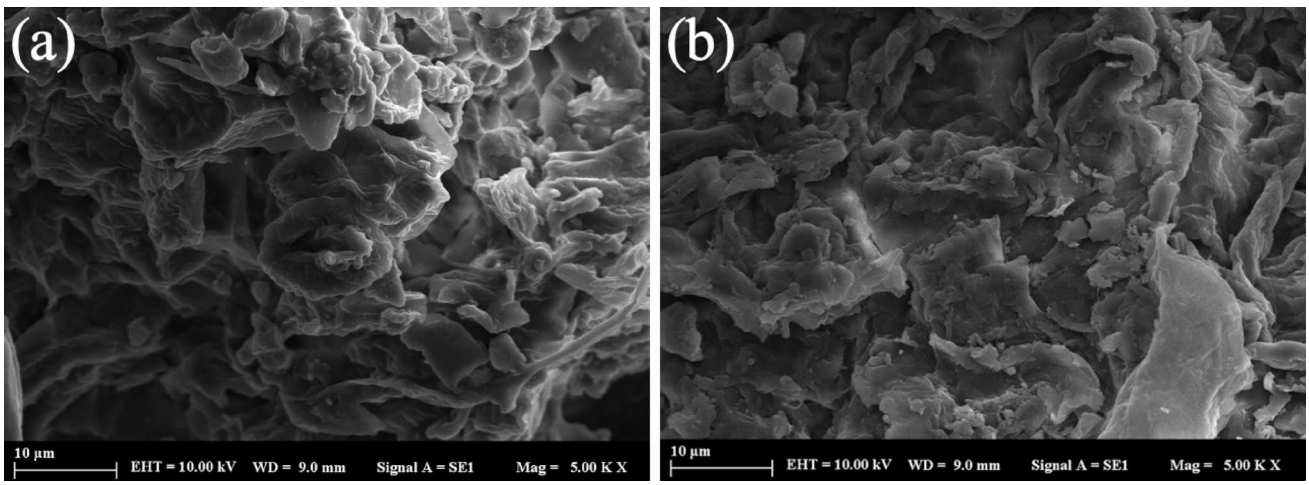

Fig. 3 The SEM images of *T. spicata* L. biomass before (**a**) and after (**b**) MB dye adsorption

possesses a pK_a value of 3.8, signifying that it mostly occurs in its cationic form (MB^{2+}) at pH levels exceeding 3.8. Consequently, in experimental conditions when the pH is about 7, the biomass surface has a negative charge, whereas MB remains entirely cationic, thereby facilitating electrostatic interactions. The pH-dependent behavior indicates that the adsorption of MB onto *T. spicata* L. biomass is significantly affected by the surface charge of the adsorbent and the ionic form of the dye, which collectively enhance adsorption via electrostatic attraction and potentially hydrogen bonding.

Zeta potential measurements were conducted to assess the electrostatic characteristics of the adsorbent surface and alterations during the adsorption process (Li et al. 2019b; Dos Santos et al. 2025). The zeta potential curves before and after adsorption were illustrated in Fig. 5. Before adsorption, the zeta potential of the *T. spicata* L. surface was measured at −27.8 mV, signifying a markedly negatively charged surface. After adsorption, the zeta potential diminished to −12.0 mV. This reduction indicates that the cationic MB molecules adhere to the surface via electrostatic interactions, partially neutralizing the surface charge. The alteration in zeta potential unequivocally indicates the effective adsorption of MB and the modification of the charge equilibrium on the adsorbent surface. Moreover, it was determined that the active spots on the surface engage with MB molecules, and the adsorption mechanism predominantly relies on electrostatic attraction.

Dye Selectivity Tests

Figure 6 displays the selectivity results as column graphs. *T. spicata* L. biomass had a markedly superior adsorption ability for cationic dyes relative to anionic dyes, as determined by dye selectivity studies conducted with distilled water (ionic strength = 0 M) at pH ≈ 7 and 298 K. Among the evaluated dyes, methylene blue (MB) exhibited significant removal efficiency, suggesting a robust contact with the biomass surface. The point of zero charge (pH_{pzc}) of the

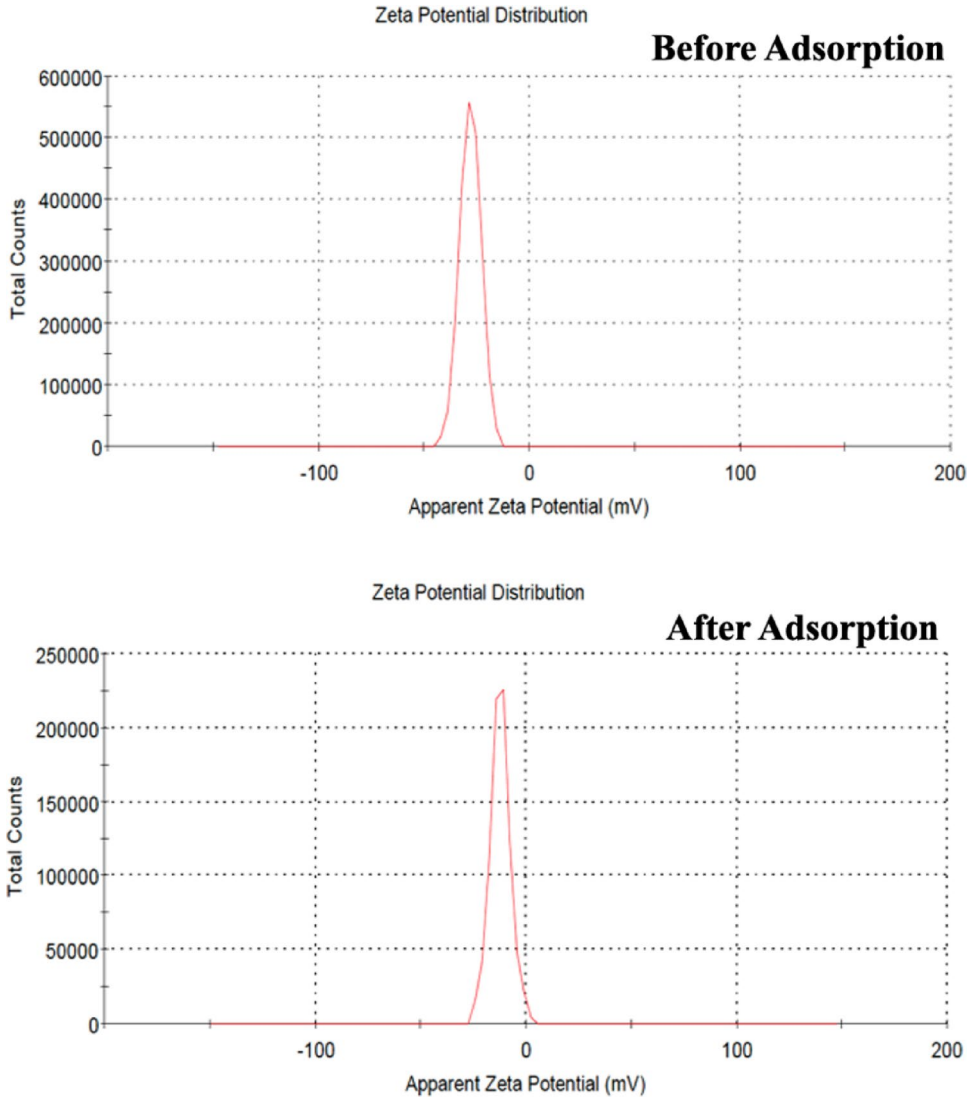

Fig. 5 The zeta potential curves of *T. spicata* L. before and after adsorption

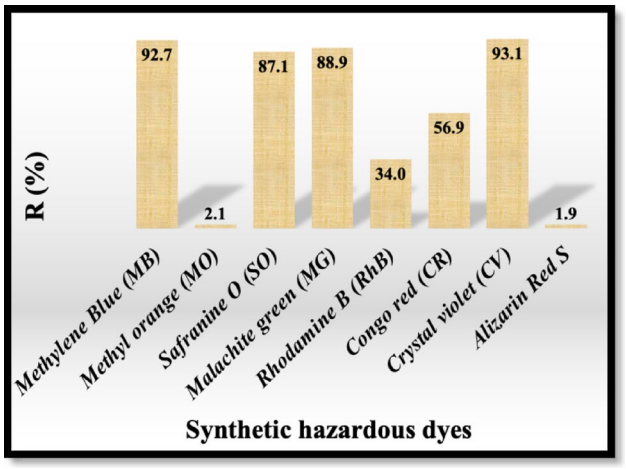

Fig. 6 The selectivity of different cationic and anionic dyes onto *T. spicata* L. biomass (agitation rate: 120 rpm, pH: 7, adsorbent dosage: 0.05 g/ 50 mL, initial concentration: 20 mg/L, contact time: 45 min, temperature: 298 K)

biomass was established at 6.50, signifying that the surface possesses a net negative charge at pH levels exceeding this value. Consequently, in experimental settings, the biomass surface exhibits a little anionic character, promoting electrostatic interaction with cationic dye molecules like MB. MB was chosen as a model dye for subsequent adsorption experiments owing to its exceptional performance in selectivity assessments, its prevalent occurrence in industrial effluents, and its thoroughly defined analytical features that enable precise monitoring of its adsorption behavior.

Taguchi Optimization and Statistical Analysis

The data from the MB dye adsorption and the five-level, four-factor orthogonal matrix were shown in Table 2, along with the S/N ratio that was determined for its analysis using Eq. (1). It is increasingly crucial to demonstrate that the ideal adsorption process is articulated and that favorable ratios were preferred for every variable the higher the S/N (Tan et al. 2017; Alex Mbachu et al. 2023).

The MB dye removal percentage as a function of S/N ratio was plotted against initial MB concentration, solution pH, contact time, and adsorbent dosage in Fig. 7. The graphs provide information on the most crucial metrics and ideal levels. 20 mg/L initial MB concentration, 8 pH, 60 min contact time, and 0.20 g/50 mL adsorbent dosage are the ideal parameter levels for maximal removal effectiveness, as indicated by the main effect graphs in Fig. 7. 95.82% removal percentages are anticipated under these ideal circumstances (S/N ratio = 39.63). The initial dye concentration and contact duration were shown to have their maximum points at

Table 2 Experimental design matrix and expected response

Run no.	Adsorption process variables				Adsorption efficiency	
	C (mg/L)	*p* (pH)	*t* (min)	*d* (g/50 mL)	*R* (%)	*S/N* ratio
1	10	2	5	0.01	25.94	28.28
2	20	2	15	0.05	36.86	31.33
3	30	2	30	0.10	58.35	35.32
4	40	2	60	0.15	69.23	36.81
5	50	2	90	0.20	79.02	37.95
6	20	4	30	0.01	51.73	34.27
7	30	4	60	0.05	88.83	38.97
8	40	4	90	0.10	92.91	39.36
9	50	4	5	0.15	90.20	39.10
10	10	4	15	0.20	95.33	39.58
11	30	8	90	0.01	67.90	36.64
12	40	8	5	0.05	74.88	37.49
13	50	8	15	0.10	88.67	38.96
14	10	8	30	0.15	95.74	39.62
15	20	8	60	0.20	95.82	39.63
16	40	10	15	0.01	53.57	34.58
17	50	10	30	0.05	85.18	38.61
18	10	10	60	0.10	94.75	39.53
19	20	10	90	0.15	95.21	39.57
20	30	10	5	0.20	93.65	39.43
21	50	12	60	0.01	64.91	36.25
22	10	12	90	0.05	92.97	39.37
23	20	12	5	0.10	90.13	39.09
24	30	12	15	0.15	93.98	39.46
25	40	12	30	0.20	94.27	39.49

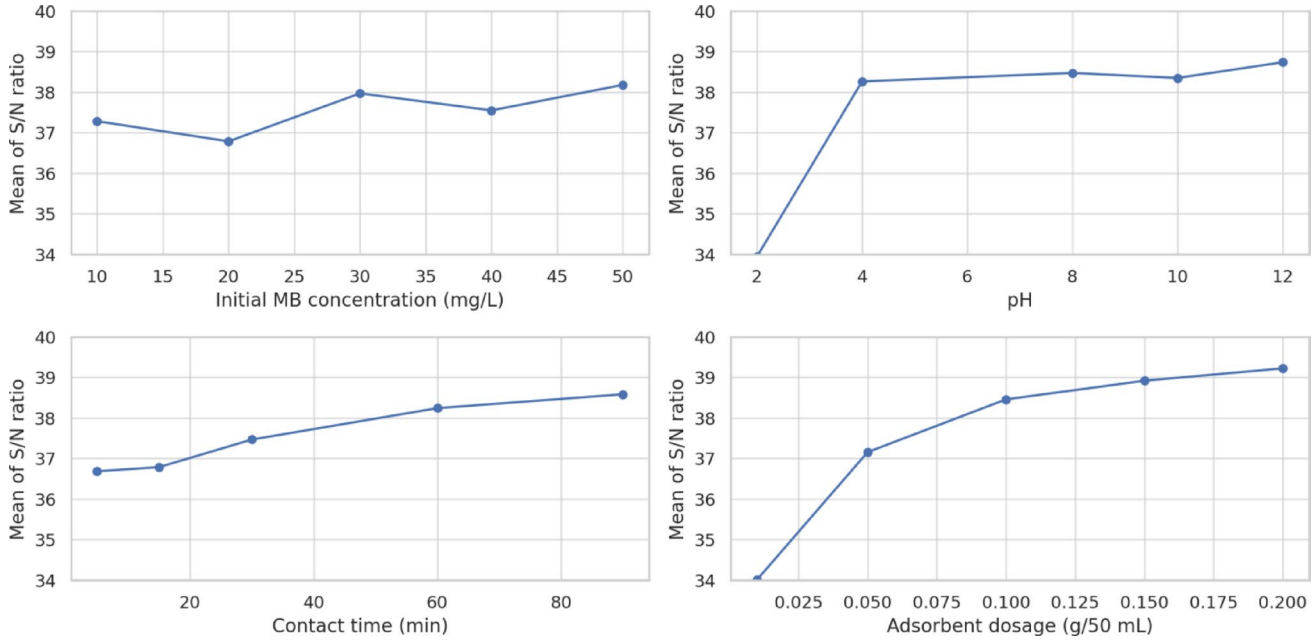

Fig. 7 The main effect of the parameter on S/N ratios for different factors: initial MB concentration, pH, contact time, and adsorbent dosage. Signal-to-Noise Ratio: The larger-The better

Table 3 Analysis of variance (ANOVA) for removal efficiency

Source	DF	Seq SS	Contribution	Adj SS	Adj MS	F-Value	*P*-Value
p	4	3919	40.28%	3919	979.9	64.80	0.000
C (mg/L)	4	208.9	2.15%	208.9	52.22	3.45	0.064
t (min)	4	533.7	5.48%	533.7	133.4	8.82	0.005
t (g/50 mL)	4	4947	50.84%	4947	1236	81.79	0.000
Error	8	121.0	1.24%	121.0	15.12		
Total	24	9731	100.0%				

low levels, whereas the adsorbent dosage and pH both reach their maximum points at high levels. This implies that high dye molecule concentration, acidic pH, and low adsorbent dosage may all have detrimental effects on the adsorption process.

The adequacy of the model was evaluated using analysis of variance (ANOVA), and the ANOVA results for adsorption efficiency are presented in Table 3. The overall significance of the model was justified based on the F-test (F-value), significance level (p-value), and the percentage of explained variance (contribution). A total of 98.76% of the variation was explained by the model factors, while only 1.24% was attributed to the error term, indicating that the model possesses a high explanatory power. Among the factors in the model, solution pH (p) and adsorbent dosage (d) were found to be statistically significant, as their p-values were less than 0.05. In particular, the adsorbent dosage, with F = 81.79 and $p = 0.000$, accounted for 50.84% of the total variation, making it the most influential parameter. pH followed as the second most effective factor, contributing 40.28% of the total variation, with F = 64.80 and $p = 0.000$. The contact time (t) was also considered significant in the model with $p = 0.005$, although its contribution was relatively lower at 5.48%, indicating a moderate effect on the adsorption process. In contrast, the initial MB concentration (C) was not statistically significant, with $p = 0.064$. The error term of the model contributed only 1.24%, which confirms the model's high accuracy and reliability.

Effect of Optimum Physicochemical Parameters

Using *T. spicata* L. biomass, the impact of adsorbent amount on the removal of MB dye from aqueous solutions was assessed in the range of 0.01 g to 0.20 g adsorbent dosage at a fixed volume of 50 mL, with a constant initial dye concentration of 20 mg/L, at 25 °C, with a stirring speed of 120 rpm, a contact time of 45 min, and a pH of roughly 7. All the findings were displayed in Fig. 8a. The R% value for MB dye was observed to increase quickly based on the amount of adsorbent at first, slowing down after 0.05 g of adsorbent, and then showing a modest increase after 0.05 g of adsorbent, as illustrated in Fig. 8a. This is because *T.*

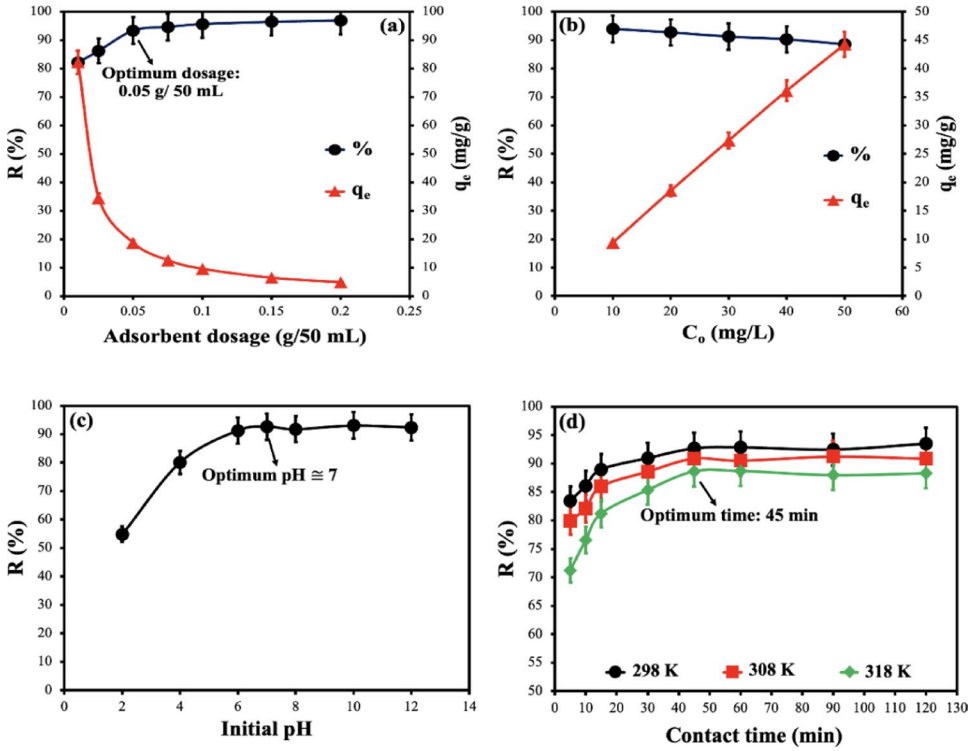

Fig. 8 The effect of physico-chemical parameters onto MB dye adsorption using *T. spicata* L. biomass: **a** adsorbent dosage (agitation rate: 120 rpm, contact time: 45 min, pH: 7, initial concentration: 20 mg/L, temperature: 298 K), **b** initial concentration (agitation rate: 120 rpm, contact time: 45 min, pH: 7, adsorbent dosage: 0.05 g/ 50 mL, temperature: 298 K), **c** initial pH (agitation rate: 120 rpm, contact time: 45 min, adsorbent dosage: 0.05 g/ 50 mL, initial concentration: 20 mg/L, temperature: 298 K), and **d** contact time (agitation rate: 120 rpm, pH: 7, adsorbent dosage: 0.05 g/ 50 mL, initial concentration: 20 mg/L)

spicata L. biomass had empty accessible active sites at first, but as the amount of adsorbent increased, more accessible active sites appeared. In addition, it was noted that the adsorption of MB dye caused the R% value to stay nearly constant at roughly 93% following the addition of 0.05 g of adsorbent. However, as Fig. 8a illustrates, it was found that as the amount of adsorbent increased, the MB dye's adsorption capacity progressively declined. The adsorption capacity dropped from 82.16 mg/g to 4.84 mg/g, according to the observation. At elevated adsorbent concentrations, despite an increase in the total number of active sites, a constant quantity of dye molecules is inadequate to saturate all available sites. This leads to a diminished dye-to-adsorbent ratio and a reduced adsorption capacity per unit mass. Augmenting the quantity of adsorbent can enhance interparticle interactions and aggregation, perhaps resulting in a diminished effective surface area and accessibility to active sites. This tendency has also been documented in the literature for various biosorbent systems (Vigneshwaran et al. 2021; Sismanoglu et al. 2023; Karadeniz et al. 2023).

Figure 8b displays the variations in MB dye's adsorption capacity and R% based on the initial concentration. Adsorption experiments were conducted using initial dye concentrations of 10, 20, 30, 40, and 50 mg/L while maintaining constant values for all other parameters. As the original concentration increased, it was discovered that the R% values fell. With an increase in the original dye concentration, the R% value of MB dye was found to decline from 93.89% to 88.48%. The reason for this is that when the dye concentration rises, the surface of *T. spicata* L. biomass becomes saturated with accessible active components. It was shown, however, that as the dye concentration increased, so did the adsorption capacity. The number of collisions between dye molecules and *T. spicata* L. biomass surface molecules increase with increasing initial dye concentration, perhaps improving the adsorption process. The adsorption capacity consequently increases (Firoozi et al. 2020).

The pH of the solution is a critical element affecting the adsorption process, as it can substantially influence the surface charge of the adsorbent and the chemical speciation of the dye molecules (Deng et al. 2019; Xiao et al. 2020; Akin et al. 2022). The pH_{pzc} for *T. spicata* L. biomass was established at 6.50, signifying that the surface acquires a negative charge at pH levels exceeding this value. MB dye possesses a pK_a value of 3.8, indicating that it mostly occurs in its cationic form (MB^{2+}) at pH levels exceeding 3.8. Consequently, at pH levels exceeding 4, the electrostatic interaction between the negatively charged biomass surface and the cationic MB molecules is promoted, thereby improving adsorption efficiency. Figure 8c demonstrates that the removal percentage (R%) of MB increased with elevated pH and stabilized beyond a specific threshold. At acidic pH values ($pH < pH_{pzc}$), adsorption effectiveness decreased due to the protonation of active sites on the biomass surface, resulting in repulsive interactions with the cationic dye. Conversely, at elevated pH levels ($pH > pH_{pzc}$), the biomass surface exhibits an increased negative charge

density, enhancing electrostatic interactions with MB^{2+} ions. Based on these data, a working pH of around 7 was chosen for the following adsorption tests to guarantee excellent performance.

It is crucial to examine how contact time affects the adsorption process to assess adsorption efficiency, carry out kinetic analyses, and identify the adsorption mechanism (Jawad et al. 2018, 2019). Depending on the contact time, Fig. 8d displays the variation in the R% value of MB dye at various temperatures. Other parameters were held constant throughout the contact time range of 0–120 min to assess the impact of contact time on the adsorption process. According to Fig. 8d, the R% value of MB dye was around 83% at the start of the adsorption process, increased as the contact duration increased, and the system reached equilibrium after about 45 min. Furthermore, the adsorption capability was discovered to vary with temperature. As the temperature rose, it was found that the MB dye's adsorption ability dropped, as shown in Fig. 8d. The MB dye adsorption process on *T. spicata* L. biomass was shown to be exothermically occurring in this instance.

Effect of Ionic Strength

Figure 9 illustrates that the inclusion of NaCl and $CaCl_2$ salts in the solution medium resulted in a significant reduction in the adsorption efficacy of MB dye on *T. spicata* L. biomass. The elimination efficiency decreased from 92.67% to 85.79% with NaCl and to 60.41% with $CaCl_2$. The decrease can be ascribed to two primary factors: (I) the competitive interaction of Na^+ and Ca^{2+} ions with the negatively charged active sites on the biomass surface, and (II) potential alterations in MB speciation resulting from the presence of chloride ions. MB may establish ionic complexes with Cl^- (e.g., $MB–Cl^-$), thereby modifying its adsorption characteristics relative to its unbound cationic form (MB^{2+}). The data indicate that electrostatic interactions and dye speciation contribute to the reduced adsorption effectiveness under elevated ionic strength settings (Pandey et al. 2020; Alver et al. 2020; Bollinger et al. 2025).

Adsorption Isotherms

Figure 10a displays the isotherm curve for the removal of MB dye using *T. spicata* L. biomass. The adsorption isotherm was found to be appropriate for the L2-type isotherm upon examining Fig. 10a. Conversely, Figs. 10b, c, and d display the non-linear graphs of the Langmuir, Freundlich, and D-R isotherm models, respectively.

Table 4 displays the estimated values of the parameters. The correlation coefficient (r^2) and different error functions were used to determine which model was the best. As a result, high correlation coefficients and somewhat reduced relative error functions show that the experimental data fit the Langmuir model effectively. In contrast, the Langmuir model yielded a q_m value of 65.03 mg/g at 298 K, suggesting that the biomass of *T. spicata* L. efficiently eliminated MB dye from wastewater. Further analysis of the K_L values derived from the Langmuir model revealed that the values fell between 0 and 1, suggesting that the adsorption process went well. In a similar vein, it was shown that the adsorption process was advantageous and that the "n" value derived from the Freundlich model fell between 1 and 10. It may be concluded that the adsorption process took place physically because the E_{D-R} value determined using the D-R isotherm model was less than 8 kJ/mol.

A comparison was made between the highest monolayer adsorption capacity of MB dye on *T. spicata* L. biomass and other documented adsorbents that were employed to remove the same adsorbate, as indicated in Table 5. With an adsorption capacity of 65.03 mg/g, *T. spicata* L. biomass was found to be comparatively high when compared to the other adsorbents listed in Table 5.

Adsorption Kinetics

Figures 11a and b display the *pseudo-first order* and *pseudo-second order* kinetic models' non-linear graphs. Table 6 presents the results of the calculation of kinetic parameters from these non-linear graphs. Additionally, Table 6 lists the error values used to assess the kinetic models' correctness and applicability. According to the results, in the instance of

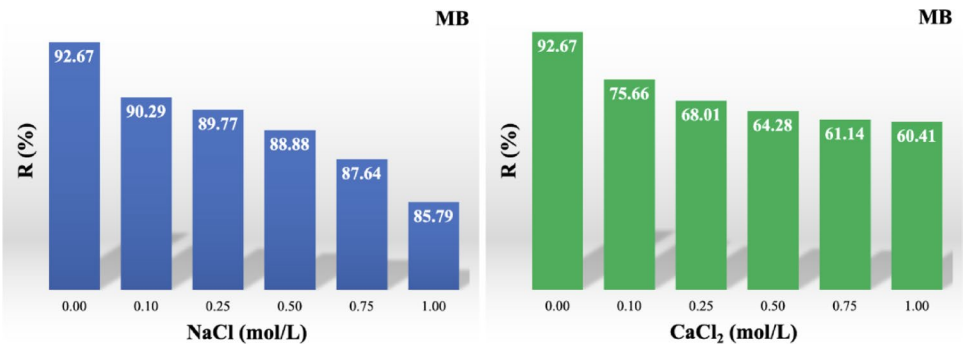

Fig. 9 The effect of ionic strength on MB adsorption performance of *T. spicata* L. biomass (agitation rate: 120 rpm, pH: 7, adsorbent dosage: 0.05 g/ 50 mL, initial concentration: 20 mg/L, contact time: 45 min, temperature: 298 K)

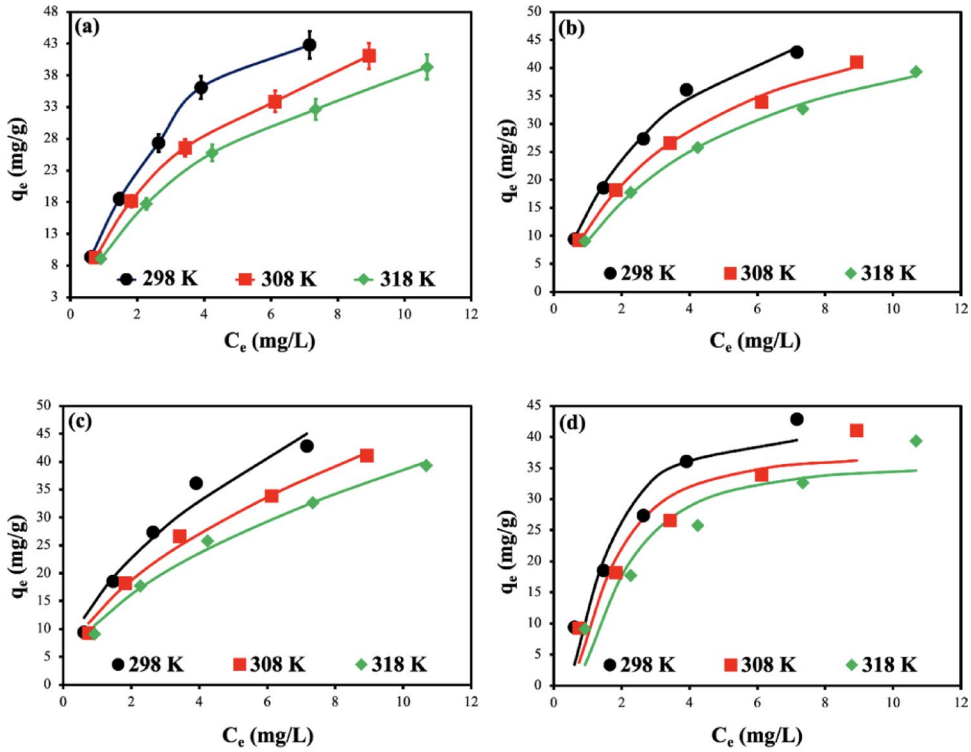

Fig. 10 The isotherm curves (**a**) and non-linear Langmuir (**b**), Freundlich (**c**), and D-R (**d**) graphs of MB dye adsorption onto *T. spicata* L. biomass (agitation rate: 120 rpm, pH: 7, adsorbent dosage: 0.05 g/ 50 mL, contact time: 45 min)

Table 4 Non-linear isotherm parameters for the adsorption of MB dye on *T. spicata* L. biomass (agitation rate: 120 rpm, pH: 7, adsorbent dosage: 0.05 g/ 50 mL, contact time: 45 min)

Temperature (K)	T. spicata L.		
	298	308	318
Langmuir isotherm			
q_m (mg/g)	65.03	59.20	57.16
K_L (L/g)	0.2847	0.2373	0.1949
SSE	4.834	2.359	1.755
ARE	2.982	2.174	2.304
RMSE	1.269	0.8867	0.7647
SD	0.9832	0.6868	0.5924
χ^2	0.1523	0.0762	0.0705
r^2	0.9991	0.9987	0.9977
Freundlich isotherm			
K_F (mg/g) · (L/g)$^{1/n}$	15.64	12.89	11.21
n	1.861	1.872	1.864
SSE	26.12	6.371	5.003
ARE	10.08	5.896	5.254
RMSE	2.950	1.457	1.291
SD	2.285	1.129	1.001
χ^2	1.139	0.4133	0.3317
r^2	0.9988	0.9988	0.9987
Dubinin-Radushkevich isotherm			
$q_{D\text{-}R}$ (mg/g)	41.31	37.54	35.80
$E_{D\text{-}R}$ (kJ/mol)	1.072	1.011	0.9012
SSE	65.92	74.63	75.72
ARE	19.06	20.18	21.09
RMSE	4.687	4.988	5.024
SD	3.631	3.863	3.891
χ^2	11.55	9.623	11.17
r^2	0.9908	0.9939	0.9932

Table 5 Various adsorbents prepared from biomass and natural materials for MB dye adsorption from wastewater

Adsorbent	q_m (mg/g)	References
T. spicata L.	65.03	This work
Poultry litter	70.32	Yusuff et al. (2021)
Spent rice	8.30	Rehman et al. (2012)
Eucalyptus sheathiana bark	45.24	Afroze et al. (2016)
Pine tree leaf	36.88	Sen (2023)
Pinus radiata L.	109.9	Sen et al. (2011)
Rhizopus oryzae	8.25	Dey et al. (2015)
Azadirachta indica	8.76	Bhattacharyya and Sharma (2005)
BC_L600	64.99	Kundu et al. (2024)
Cocos nucifera L.	112.4	Jawad et al. (2016)

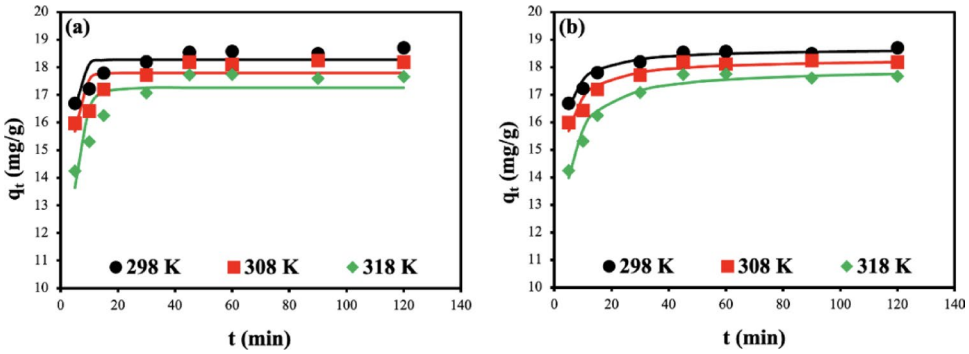

Fig. 11 The non-linear *pseudo-first-order* (**a**) and *pseudo-second-order* (**b**) kinetic curves of MB dye adsorption onto *T. spicata* L. biomass

Table 6 Non-linear kinetic parameters for the adsorption of MB dye on *T. spicata* L. biomass (agitation rate: 120 rpm, pH: 7, adsorbent dosage: 0.05 g/ 50 mL, initial concentration: 20 mg/L)

Temperature (K)	T. spicata L.		
	298	308	318
Pseudo-first-order			
k_1 (min^{-1})	0.4681	0.4263	0.3119
q_e (cal) (mg/g)	18.27	17.80	17.26
q_e (exp) (mg/g)	18.53	18.18	17.73
SSE	1.418	2.266	3.281
ARE	1802	1749	1669
RMSE	0.6876	0.8691	1.046
SD	0.3766	0.4761	0.5728
χ^2	0.0782	0.1291	0.2001
r^2	0.9999	0.9999	0.9999
Pseudo-second-order			
k_2 (g/mg.min)	0.0808	0.0655	0.0390
q_e (cal) (mg/g)	18.68	18.29	17.96
q_e (exp) (mg/g)	18.53	18.18	17.73
SSE	0.1857	0.3947	0.4277
ARE	1803	1750	1670
RMSE	0.2488	0.3627	0.3776
SD	0.1363	0.1987	0.2068
χ^2	0.0106	0.0234	0.0267
r^2	0.9999	0.9999	0.9999

pseudo-first order kinetics, the predicted and experimental results did not coincide. Furthermore, the *pseudo-second order* kinetic model was shown to be more appropriate for describing the adsorption process due to its higher correlation values and smaller error functions. This result implied that MB dye adsorption took place by a chemisorption interaction (Ullah et al. 2025).

Possible Adsorption Mechanism

The adsorption process of MB dye onto *T. spicata* L. biomass was clarified using FTIR-ATR spectral analysis, adsorption isotherm and kinetic modeling, and zeta potential measurements. The possible adsorption mechanism was illustrated in Fig. 12. FTIR-ATR spectra demonstrated alterations in the vibrational bands associated with –COOH, –OH, and $–NH_2$ functional groups, signifying their involvement in MB binding. These polar groups presumably enhance adsorption via hydrogen bonding and electrostatic interactions. The investigation of zeta potential further corroborated the interaction mechanism. The biomass surface displayed a zeta potential of -27.8 mV before adsorption, which diminished to -12.0 mV following MB absorption. The reduction in surface charge corroborates the electrostatic interaction between the negatively charged biomass and cationic methylene blue molecules (MB^{2+}). Cationic MB molecules dominate at pH≥4, as the pK_a value of MB is 3.8. The adsorption energy derived using the D-R isotherm model was less than 8 kJ/mol, signifying that the process was predominantly physical. The *pseudo-second order* kinetic model, which posits that the rate-limiting phase entails valence forces via electron sharing or exchange, generally indicates chemisorption. This apparent conflict can be reconciled by recognizing that the pseudo-second-order

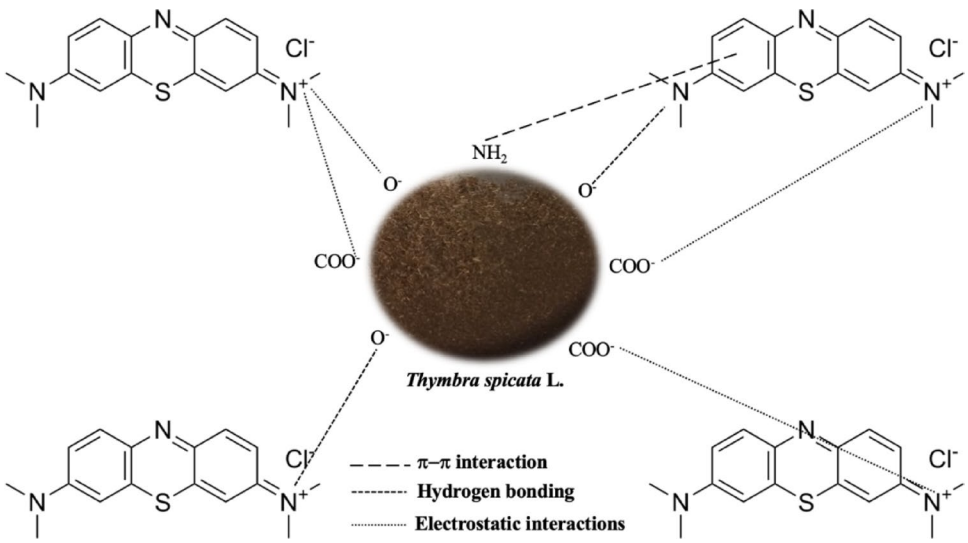

Fig. 12 The possible mechanism of MB dye adsorption onto *T. spicata* L. biomass

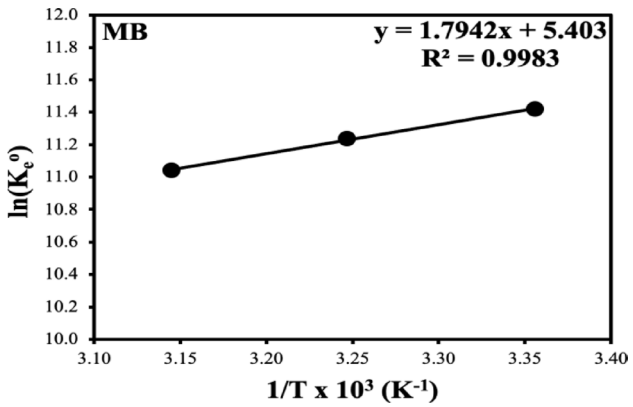

Fig. 13 The linear Van't Hoff plot of MB dye adsorption onto *T. spicata* L. biomass

model can also characterize systems whose surface contacts are robust, albeit not exclusively covalent. In this instance, adsorption is predominantly influenced by physical forces, including electrostatic attraction and hydrogen bonding, with potential contributions from π–π interactions between the aromatic rings of methylene blue and the lignocellulosic constituents of the biomass. Moreover, the influence of ionic strength, examined through NaCl and $CaCl_2$ tests, underscored the significance of electrostatic interactions in the overall mechanism, illustrating that competing cations and chloride ions disrupt MB adsorption. The adsorption of MB onto *T. spicata* L. biomass is a complex process characterized by physical adsorption, electrostatic attraction, hydrogen bonding, and π–π interactions, influenced by pH and the ionic composition of the solution.

Adsorption Thermodynamics

The calculation of the thermodynamic equilibrium constant (K_e^o) was done with Eq. (10). Figure 13 displays the linear Van't Hoff graph that was created between $1/T$ and $\ln K_e^o$ values in accordance with Eq. (11). The enthalpy and entropy values, which were shown in Table 7, were determined using the linear graph's slope and intercept, respectively. Furthermore, adsorption Gibbs free energy values were computed using Eq. (12), and Table 7 presents the findings. Table 7 shows that an exothermic adsorption process is indicated by a negative enthalpy value. An analysis of the entropy value revealed that the surface disorder was high. The analysis of the Gibbs free energy values revealed that the adsorption process was spontaneous because the values were negative.

Recycling of *T. spicata* L

The recyclability of adsorbents is essential for their effective use in wastewater treatment (Wu et al. 2023; Tohdee et al. 2024; Jarodhia et al. 2025). A 20 mg/L MB solution was chosen for the adsorption cycle experiment, and the recycling efficacy of *T. spicata* L. biomass was examined. Following each adsorption cycle, desorption was conducted using a 0.5 M HCl solution, and the findings were recorded after seven rounds of adsorption-desorption tests. Figure 14 illustrates that the first removal rate of MB by *T. spicata* L. biomass was 92.67%. Following seven experimental cycles, the removal rate of MB by *T. spicata* L. biomass exhibited

Table 7 Thermodynamic parameters for the adsorption of MB dye on *T. spicata* L. biomass

Thermodynamic parameters	ΔH^o (kJ/mol)	ΔS^o $(J/mol.K)$	ΔG^o (kJ/mol)		
			25 °C	35 °C	45 °C
Thymbra spicata L.	-14.92	44.92	-28.31	-28.75	-29.20

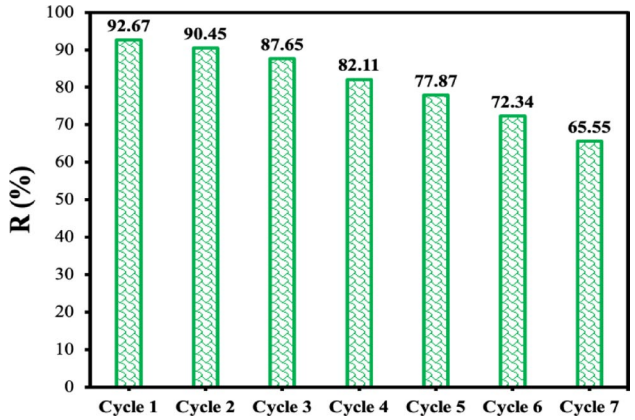

Fig. 14 The reusability of *T. spicata* for MB dye removal

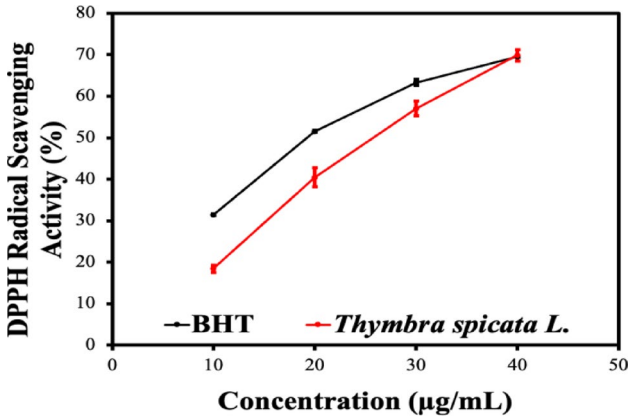

Fig. 15 The DPPH radical scavenging activity of *T. spicata* L. extract

a little decline, remaining at 62.55%. The findings indicated that *T. spicata* L. biomass can be utilized frequently for the elimination of MB and analogous dyes from wastewater.

Total Phenolic Content

Without encouraging additional oxidative processes, phenolic substances can scavenge reactive oxygen intermediates. Phenolic compounds transfer electrons to phosphomolybdic/phosphotungstic acid complexes in an alkaline medium, forming blue complexes that can be detected spectroscopically at about 760 nm (Ainsworth and Gillespie 2007). The total phenolic content of the water extract of *T. spicata* L. biomass was found to be 93.32±1.23 µg pyrocatechol equivalents per mg extract. This shows that *T. spicata* L. biomass has a good amount of phenolic compounds, which have antioxidant properties.

In the literature, Gumus et al. reported that the total phenolic content of the methanol extract of *T. spicata* aerial parts was 75.19±1.3 mg gallic acid equivalent (GAE) per g extract (Gumus et al. 2011). Khalil et al. reported that aqueous extract of *T. spicata* contained 150±3.7 and ethanol extract contained 250±6.9 mg GAE/g dry extract of total phenolic content (Khalil et al. 2019). In the study by Gedikoglu et al., the total phenolic content of 80% methanol and 80% ethanol extracts of *T. spicata* was reported as 13.15±0.135 and 13.13±0.249 mg GAE/dry weight, respectively (Gedikoglu et al. 2019). Ozcan and Ozkan prepared different extracts by using different solvents and extraction methods and found that total phenolic contents were 4.52–163.10 mg GAE/g (Ozcan and Ozkan 2018). In the study by Llorent-Martínez et al., the methanol extract of *T. capitata* had a total phenolic content of 127.52±4.32 mg GAE/g, and the infusion had a total phenolic content of 94.57±0.83 mg GAE/g (Llorent-Martínez et al. 2022). The results we obtained are consistent with the results in the literature and show that different extracts of *T. spicata* contain phenolic compounds. Different solvents or different extraction techniques might be some of the reasons for differences in the results.

DPPH Radical Scavenging Activity

The extract's capacity to reduce DPPH has been used to investigate its antioxidant properties. The basis for this interaction is the transfer of an electron or a hydrogen atom to the DPPH radical from the antioxidant compound. Reduction results in discoloration from purple to pale yellow, indicating scavenging action (Hussen and Endalew 2023). Results of the DPPH radical scavenging activity were given in Fig. 15. Results show that *T. spicata* L. biomass had DPPH scavenging activity at all tested concentrations. While at 10 µg/mL the activity was 18.42±0.82%, activity was increased with increasing concentrations to eventually 69.89±1.36% at 40 µg/mL. At the same concentrations, BHT had 31.42±0.17–69.49±0.03% scavenging activity, which shows *T. spicata* L. biomass had similar activity to BHT at the same concentrations.

It was reported by Gumus et al. that the DPPH radical scavenging activity of the methanol extract of *T. spicata* at 0.25 mg/mL concentration was around 40%, and at 0.5 mg/mL concentration, it was around 80% (Gumus et al. 2011). In Khalil et al.'s study, IC_{50} for DPPH activity of aqueous extract of *T. spicata* was reported as 28.5±1.28 µg/mL, and for ethanol extract it was 24.5±1.09 µg/mL (Khalil et al. 2019). *T. spicata*'s 80% methanol extract had an IC_{50} of 35.28±0.45, and the 80% ethanol extract had an IC_{50} of 43.9±0.845 µg/mL (Gedikoglu et al. 2019). The IC_{50} of DPPH radical scavenging activity results of *T. spicata* extracts by Ozcan and Ozkan were given as 572.60–1035.6 µg/mL (Ozcan and Ozkan 2018). Methanol extract of *T. capitata* had DPPH activity of 269.71±0.63 mg Trolox equivalent (TE)/g, and the infusion's activity was 259.63±0.62 mg TE/g (Llorent-Martínez et al. 2022).

Although the results are similar to those in the literature, it might be said that the activity of the water extract of T. spicata is better than that of other extracts.

Total Antioxidant Capacity

The phosphomolybdate assay determines the ability of an extract to eliminate a free radical by transferring an electron. The extract's total antioxidant capacity was determined by reducing molybdate (VI) to molybdate (V) (Hussen and Endalew 2023). The results show that the water extract of *T. spicata* L. had a total antioxidant capacity of 177.89 ± 3.20 µg ascorbic acid equivalents (AAE) per mg extract.

In the study by Gumus et al., it was reported that the methanol extract of *T. spicata*'s total antioxidant activity was 216.80 ± 0.0 mg AAE per g extract (Gumus et al. 2011). In the study by Ozcan and Ozkan, the total antioxidant capacity of *T. spicata*'s different extracts was reported as 42.31-101.52 mg AAE/g (Ozcan and Ozkan 2018). While the total antioxidant capacity of the methanol extract of *T. capitata* was reported by Llorent-Martínez et al. as 3.61 ± 0.27 mmol TE/g, for the infusion, it was 2.57 ± 0.08 mmol TE/g (Llorent-Martínez et al. 2022).

β-Carotene Bleaching Assay

In the β-carotene bleaching assay, the absence of an antioxidant causes rapid discoloration. The abstraction of a hydrogen atom creates a linoleic acid free radical that attacks the unsaturated β-carotene molecule. As a result, β-carotene oxidizes and breaks down, losing its chromophore and distinctive orange color, which is monitored spectrophotometrically (Amiri 2012). At 1 mg/mL concentration, the extract had 0.96 ± 0.01 for 60 min and 0.94 ± 0.03 for 120 min activity compared to BHT (1.00). This shows that the extract had very similar activity to BHT to protect β-carotene.

Conclusions

This work illustrated the efficient application of *T. spicata* L. biomass as a natural, economical, and sustainable adsorbent for the extraction of MB dye from aqueous solutions, in accordance with zero-waste and circular economy principles. Compared to conventional water treatment technologies, the use of plant-derived adsorbents, such as *T. spicata* L. biomass, offers several advantages. Plant-based biosorbents are generally cost-effective, renewable, biodegradable, and readily available, making them an attractive option for sustainable and localized water treatment solutions. Furthermore, the utilization of such biomass promotes the principles of a circular economy by enabling the repurposing of agricultural or plant waste. The Taguchi approach was employed to optimize the adsorption process, demonstrating that solution pH, adsorbent dosage, initial dye concentration, and contact duration substantially affected the removal effectiveness. The adsorption mechanism was clarified via equilibrium and kinetic modeling. The Langmuir isotherm model exhibited the optimal fit for the experimental data, signifying monolayer adsorption on a uniform surface, with a maximum adsorption capacity (q_m) of 65.03 mg/g. The *pseudo-second order* kinetic model effectively characterized the adsorption behavior, indicating that the rate-limiting phase may involve chemisorption or surface-specific interactions. FTIR-ATR examination verified the participation of functional groups including –OH, –COOH, and $–NH_2$ in the adsorption process, corroborating the existence of electrostatic interactions, hydrogen bonding, and π–π stacking. The impact of ionic strength underscored the significance of electrostatic forces and potential dye speciation consequences. In addition to its adsorption capacity, *T. spicata* L. biomass demonstrated antioxidant capabilities, suggesting its potential as a multifunctional material for environmental applications. The work advances the creation of sustainable, effective, and reusable biosorbents for wastewater treatment.

Author Contributions All authors contributed to the study conception and design. All authors read and approved the final manuscript.

Funding Open access funding provided by the Scientific and Technological Research Council of Türkiye (TÜBİTAK). No applicable.

Data Availability The data that support the findings of this study are available from the corresponding author upon reasonable request.

Declarations

Conflict of Interest The authors have no relevant financial or non-financial interests to disclose.

Ethical Approval Not applicable.

Consent to Participate Not applicable.

Consent for Publication Not applicable.

Open Access This article is licensed under a Creative Commons Attribution 4.0 International License, which permits use, sharing, adaptation, distribution and reproduction in any medium or format, as long as you give appropriate credit to the original author(s) and the source, provide a link to the Creative Commons licence, and indicate if changes were made. The images or other third party material in this article are included in the article's Creative Commons licence, unless indicated otherwise in a credit line to the material. If material is not included in the article's Creative Commons licence and your intended use is not permitted by statutory regulation or exceeds the permitted use, you will need to obtain permission directly from the copyright

holder. To view a copy of this licence, visit http://creativecommons.org/licenses/by/4.0/.

References

Abou Taleb MF, Aljowni MA, Parveen H, Mukhtar S (2025) Green coagulation and flocculation: scenedesmus algal extract-loaded chitosan/poly(vinyl alcohol) cryogel for effective water treatment. Int J Biol Macromol 290:138739

Afroze S, Sen TK, Ang HM (2016) Adsorption performance of continuous fixed bed column for the removal of methylene blue (MB) dye using *Eucalyptus sheathiana* bark biomass. Res Chem Intermed 42:2343–2364

Ainsworth EA, Gillespie KM (2007) Estimation of total phenolic content and other oxidation substrates in plant tissues using Folin–Ciocalteu reagent. Nat Protoc 2:875–877

Akgul I, Isik B, Ugraskan V (2024) Preparation and characterization of oat hulls-filled-sodium alginate biocomposite microbeads for the effective adsorption of toxic methylene blue dye. Int J Biol Macromol 280:135800

Akin K, Ugraskan V, Isik B, Cakar F (2022) Adsorptive removal of crystal violet from wastewater using sodium alginate-gelatin-montmorillonite ternary composite microbeads. Int J Biol Macromol 223:543–554

Al Kausor M, Sen Gupta S, Bhattacharyya KG, Chakrabortty D (2022) Montmorillonite and modified montmorillonite as adsorbents for removal of water soluble organic dyes: a review on current status of the art. Inorg Chem Commun 143:109686

Alahmad J, BiBi A, Al-Ghouti MA (2024) Application of TiO_2-loaded fly ash-based geopolymer in adsorption of methylene blue from water: waste-to-value approach. Groundw Sustain Develop 25:101138

Alex Mbachu C, Kamoru Babayemi A, Chinedu Egbosiuba T, Ike JI, Ani IJ, Mustapha S (2023) Green synthesis of iron oxide nanoparticles by Taguchi design of experiment method for effective adsorption of methylene blue and methyl orange from textile wastewater. Res Eng 19:101198

Ali Khan M, Govindasamy R, Ahmad A, Siddiqui MR, Alshareef SA, Hakami AAH, Rafatullah M (2021) Carbon based polymeric nanocomposites for dye adsorption: synthesis, characterization, and application. Polymers 13:419

Aljeboree AM, Alkaim AF, Alsultany FH, Issa SK (2025) Highly reusable nano adsorbent based on clay-incorporated hydrogel nanocomposite for cationic dye adsorption. J Inorg Organomet Polym 35:1165–1186

Alkhouzaam A, Khraisheh M (2024) Towards sustainable management of end-of-life membranes: novel transformation of end of life (EoL) reverse osmosis membranes for efficient dye/salt separation. Desalination 571:117104

Alver E, Metin AU, Brouers F (2020) Methylene blue adsorption on magnetic alginate/rice husk bio-composite. Int J Biol Macromol 154:104–113

Amiri H (2012) Essential oils composition and antioxidant properties of three *Thymus* species. Evidence-Based Complement Alt Med 2012:1–8

Assouani A, Dabagh A, Abali M, Mahmoudy G, EL-Habacha M, Chiban M, Alahiane N, Fdil F, Sinan F, Zerbet M (2024) Evaluation of the physicochemical and bacteriological quality of groundwater in the Nihit rural commune of the Moroccan Anti-Atlas. Desalin Water Treat 317:100038

Astuti W, Chafidz A, Al-Fatesh AS, Fakeeha AH (2021) Removal of lead (Pb(II)) and zinc (Zn(II)) from aqueous solution using coal fly ash (CFA) as a dual-sites adsorbent. Chin J Chem Eng 34:289–298

Astuti W, Sulistyaningsih T, Prastiyanto D, Rusiyanto, Lanjar, Riayanti FI, Astuti AW, Wibowo WT, Handayani AD, Wulandari DA (2024) Influence of lignocellulosic composition in biomass waste on the microstructure and dye adsorption characteristics of microwave-assisted $ZnCl_2$ activated carbon. Biomass Conv Bioref 14:16681–16697

Badawi AK, Kriaa K, Osman RM, Hassan R (2024) Modified rice husk waste-based filter for wastewater treatment: pilot study and reuse potential. Chem Eng Technol 47:968–975

Bellaj M, Aziz K, El Achaby M, El Haddad M, Gebrati L, Kurniawan TA, Chen Z, Yap PS, Aziz F (2024) Cationic and anionic dyes adsorption from wastewater by clay-chitosan composite: an integrated experimental and modeling study. Chem Eng Sci 285:119615

Benhalima T, Sadi A, Dairi N, Ferfera-Harrar H (2024) Multifunctional carboxymethyl cellulose-dextran sulfate/AgNPs@zeolite hydrogel beads for basic red 46 and methylene blue dyes removal and water disinfection control. Sep Purif Technol 342:127001

Berkane N, Meziane S, Aziri S (2020) Optimization of Congo red removal from aqueous solution using Taguchi experimental design. Sep Sci Technol 55:278–288

Bhattacharyya K, Sharma A (2005) Kinetics and thermodynamics of methylene blue adsorption on Neem leaf powder. Dyes Pigm 65:51–59

Bollinger J-C, Lima EC, Mouni L, Salvestrini S, Tran HN (2025) Molecular properties of methylene blue, a common probe in sorption and degradation studies: a review. Environ Chem Lett 23:1403–1424

Boyatzis SC, Velivasaki G, Malea E (2016) A study of the deterioration of aged parchment marked with laboratory iron gall inks using FTIR-ATR spectroscopy and micro hot table. Herit Sci 4:13

Braish AG, Hassan AF, El-Essawy SA, El-Tahawy MMT (2024) Fabrication of nanozeolite-Y/chitosan composite based on rice husks for efficient adsorption of methylene blue dye: kinetic and thermodynamic studies. Adsorption 30:1643–1661

Brand-Williams W, Cuvelier ME, Berset C (1995) Use of a free radical method to evaluate antioxidant activity. LWT - Food Sci Technol 28:25–30

Bruni R, Muzzoli M, Ballero M, Loi MC, Fantin G, Poli F, Sacchetti G (2004) Tocopherols, fatty acids and sterols in seeds of four Sardinian wild Euphorbia species. Fitoterapia 75:50–61

Chkirida S, Zari N, Achour R, Hassoune H, Lachehab A, Qaiss AK, Bouhfid R (2021) Highly synergic adsorption/photocatalytic efficiency of alginate/bentonite impregnated TiO_2 beads for wastewater treatment. J Photochem Photobiol A: Chem 412:113215

Choudhary M, Kumar R, Neogi S (2020) Activated biochar derived from *Opuntia ficus-indica* for the efficient adsorption of malachite green dye, Cu^{+2} and Ni^{+2} from water. J Hazard Mater 392:122441

Chowdhury S, Dhawane SH, Jha B, Pal S, Sagar R, Hossain A, Halder G (2021) Biodiesel synthesis from transesterified *Madhuca indica* oil by waste egg shell–derived heterogeneous catalyst: parametric optimization by Taguchi approach. Biomass Conv Bioref 11:1171–1181

Chu KH, Hashim MA, Hayder G, Bollinger J-C (2024) Comparative evaluation of the Dubinin–Radushkevich isotherm and its variants. Ind Eng Chem Res 63:15002–15011

Dbik A, Bentahar S, El Khomri M, El Messaoudi N, Lacherai A (2020) Adsorption of Congo red dye from aqueous solutions using tunics of the corm of the saffron. Mater Today: Proc 22:134–139

Deng H, Mao Z, Xu H, Zhang L, Zhong Y, Sui X (2019) Synthesis of fibrous $LaFeO_3$ perovskite oxide for adsorption of Rhodamine B. Ecotoxicol Environ Saf 168:35–44

Dey MD, Shukla R, Bordoloi NK, Doley R, Mukhopadhyay R (2015) Mechanism of adsorptive removal of methylene blue using dried biomass of rhizopus oryzae. Appl Biochem Biotechnol 177:541–555

Ding L, Shao P, Luo Y, Yin X, Yu S, Fang L, Yang L, Yang J, Luo X (2020) Functionalization of UiO-66-NH_2 with rhodanine via amidation: towarding a robust adsorbent with dual coordination sites for selective capture of Ag(I) from wastewater. Chem Eng J 382:123009

Dos Santos JAP, Pires NDR, Loiola AR, Do Nascimento RF (2025) New insights into the removal of indigo blue dye from aqueous effluent using a low-cost adsorbent. Colloids Surf A: Physicochem Eng Asp 711:136338

El-Habacha M, Lagdali S, Dabagh A, Mahmoudy G, Assouani A, Benjelloun M, Miyah Y, Iaich S, Chiban M, Zerbet M (2024) High efficiency of treated-phengite clay by sodium hydroxide for the Congo red dye adsorption: optimization, cost estimation, and mechanism study. Environ Res 259:119542

Elkatory MR, Yılmaz M, Hassaan MA, El Nemr A (2024) Fabrication of date palm kernel biochar-sulfur (DPKB-S) for super adsorption of methylene blue dye from water. Sci Rep 14:6830

Erci F, Cakir-Koc R, Isildak I (2018) Green synthesis of silver nanoparticles using *Thymbra spicata* L. *var. spicata* (zahter) aqueous leaf extract and evaluation of their morphology-dependent antibacterial and cytotoxic activity. Artif Cells Nanomed Biotechnol 46:150–158

Firoozi M, Rafiee Z, Dashtian K (2020) New MOF/COF hybrid as a robust adsorbent for simultaneous removal of auramine O and rhodamine B dyes. ACS Omega 5:9420–9428

Freundlich H (1906) Over the adsorption in solution. J Phys Chem 57:385–471

Gedikoglu A, Sokmen M, Civit A (2019) Evaluation of *Thymus vulgaris* and *Thymbra spicata* essential oils and plant extracts for chemical composition, antioxidant, and antimicrobial properties. Food Sci Nutrit 7:1704–1714

Goswami R, Mishra A, Mishra PK, Rajput A (2024) Linear and nonlinear regression modelling of industrial dye adsorption using nanocellulose@chitosan nanocomposite beads. Int J Biol Macromol 274:133512

Gumus T, Albayrak S, Sagdic O, Arici M (2011) Effect of gamma irradiation on total phenolic contents and antioxidant activities of *Satureja hortensis, Thymus vulgaris*, and *Thymbra spicata* from Turkey. Int J Food Prop 14:830–839

Han X, Wang W, Ma X (2011) Adsorption characteristics of methylene blue onto low cost biomass material lotus leaf. Chem Eng J 171:1–8

Haydari I, Aziz K, Kaya S, Dastan T, Ouazzani N, Mandi L, Aziz F (2023) Green synthesis of reduced graphene oxide and their use on column adsorption of phenol from olive mill wastewater. Process Saf Environ Prot 170:1079–1091

Heidarinejad Z, Dehghani MH, Heidari M, Javedan G, Ali I, Sillanpaa M (2020) Methods for preparation and activation of activated carbon: a review. Environ Chem Lett 18:393–415

Hejji L, Aoulad El Hadj Ali Y, Azzouz A, Raza N, Villarejo LP, Kailasa SK (2024) Recent insights into molecularly imprinted membrane technology for removal of pollutants from environmental water: from organic molecules to metal ions. J Water Process Eng 58:104852

Hussen EM, Endalew SA (2023) In vitro antioxidant and free-radical scavenging activities of polar leaf extracts of *Vernonia amygdalina*. BMC Complement Med Ther 23:146

Imessaoudene A, Cheikh S, Hadadi A, Hamri N, Bollinger JC, Amrane A, Tahraoui H, Manseri A, Mouni L (2023) Adsorption performance of zeolite for the removal of congo red dye: factorial design experiments, kinetic, and equilibrium studies. Separations 10:57

Isik B (2023) Adsorptive removal of congo red and methylene blue dyes from aqueous solutions by *Rumex obtusifolius* roots. Korean J Chem Eng 40:3003–3016

Isik B (2025) Adsorptive removal of hazardous rhodamine B dye from aqueous solutions by St. John's wort (*Hypericum perforatum*). Biomass Conv Bioref 15:9553–9564

Isik B, Avci S, Cakar F, Cankurtaran O (2023a) Adsorptive removal of hazardous dye (crystal violet) using bay leaves (*Laurus nobilis* L.): surface characterization, batch adsorption studies, and statistical analysis. Environ Sci Pollut Res 30:1333–1356

Isik B, Cakar F, Cankurtaran O (2023b) Valorization of *Urtica dioica* roots as a highly-effective and eco-friendly biosorbent for adsorptive removal of hazardous textile dyes. Mater Sci Eng: B 293:116451

Isik B, Ugraskan V, Cakar F, Yazici O (2024) A comparative study on the adsorption of toxic cationic dyes by Judas tree (*Cercis siliquastrum*) seeds. Biomass Conv Bioref 14:6709–6723

Jamali GA, Devrajani SK, Memon SA, Qureshi SS, Anbuchezhiyan G, Mubarak NM, Shamshuddin SZM, Siddiqui MTH (2024) Holistic insight mechanism of ozone-based oxidation process for wastewater treatment. Chemosphere 359:142303

Jarodhia N, Joshi K, Kumar NS, Ameta KL (2025) Remediation of methylene blue dye from an aqueous solution using biomass-based nanocomposites. Biomass Conv Bioref 15:15241–15260

Jawad AH, Rashid RA, Mahmuod RMA, Ishak MAM, Kasim NN, Ismail K (2016) Adsorption of methylene blue onto coconut (*Cocos nucifera*) leaf: optimization, isotherm and kinetic studies. Desalin Water Treat 57:8839–8853

Jawad AH, Rashid RA, Ishak MAM, Ismail K (2018) Adsorptive removal of methylene blue by chemically treated cellulosic waste banana (*Musa sapientum*) peels. J Taibah Univ Sci 12:809–819

Jawad AH, Razuan R, Appaturi JN, Wilson LD (2019) Adsorption and mechanism study for methylene blue dye removal with carbonized watermelon (*Citrullus lanatus*) rind prepared via one-step liquid phase H_2SO_4 activation. Surf Interf 16:76–84

Jawad AH, Saud Abdulhameed A, Wilson LD, Syed-Hassan SSA, ALOthman ZA, Khan MR (2021) High surface area and mesoporous activated carbon from KOH-activated dragon fruit peels for methylene blue dye adsorption: optimization and mechanism study. Chin J Chem Eng 32:281–290

Karadeniz SC, Isik B, Ugraskan V, Cakar F (2023) Adsorptive removal of Safranine T dye from aqueous solutions using sodium alginate–*Festuca arundinacea* seeds bio–composite microbeads. Int J Biol Macromol 248:125880

Karmakar B, Dhawane SH, Halder G (2018) Optimization of biodiesel production from castor oil by Taguchi design. J Environ Chem Eng 6:2684–2695

Khalil M, Khalifeh H, Baldini F, Salis A, Damonte G, Daher A, Voci A, Vergani L (2019) Antisteatotic and antioxidant activities of *Thymbra spicata* L. extracts in hepatic and endothelial cells as in vitro models of non-alcoholic fatty liver disease. J Ethnopharm 239:111919

Kilic T (2006) Analysis of essential oil composition of *Thymbra spicata var. spicata*: antifungal, antibacterial and antimycobacterial activities. Z Natur C 61:324–328

Kundu D, Sharma P, Bhattacharya S, Gupta K, Sengupta S, Shang J (2024) Study of methylene blue dye removal using biochar derived from leaf and stem of *Lantana camara* L. Carbon Res 3:22

Lamberti E, Viscusi G, Kiani A, Boumezough Y, Acocella MR, Gorrasi G (2024) Efficiency of dye adsorption of modified biochar: a comparison between chemical modification and ball milling assisted treatment. Biomass Bioenergy 185:107247

Langmuir I (1918) The adsorption of gases on plane surfaces of glass, mica and platinum. J Am Chem Soc 40:1361–1403

Li G, Ye J, Fang Q, Liu F (2019a) Amide-based covalent organic frameworks materials for efficient and recyclable removal of heavy metal lead (II). Chem Eng J 370:822–830

Li T, Huang P, Liao T, Guo J, Yu X, Han B, Peng L, Zhu Y, Zhang Y (2019b) Magnetic polymer–supported adsorbent with two functional adsorption sites for phosphate removal. Environ Sci Pollut Res 26:33269–33280

Li K, Wu J, Li X, Li B, Zhou D (2024) Preparation of porous composite hydrogel with ultra-high dye adsorption capacity based on biochar: adsorption behaviors and mechanisms. Chem Eng Sci 295:120115

Lima EC, Hosseini-Bandegharaei A, Moreno-Piraján JC, Anastopoulos I (2019) A critical review of the estimation of the thermodynamic parameters on adsorption equilibria. wrong use of equilibrium constant in the Van't Hoof equation for calculation of thermodynamic parameters of adsorption. J Mol Liq 273:425–434

Liu Z, Huang X, Miao Y, Gao B, Shi Y, Zhao J, Tan SH (2022) Eggplant biomass based porous carbon for fast and efficient dye adsorption from wastewater. Ind Crops Prod 187:115510

Llorent-Martínez EJ, Ruiz-Medina A, Zengin G, Ak G, Jugreet S, Mahomoodally MF, Emre G, Orlando G, Libero ML, Bilofar, Acquaviva A, Di Simone SC, Menghini L, Ferrante C, Brunetti L, Recinella L, Leone S, Shariati MA, Uba AI, Chiavaroli A (2022) New biological and chemical evidences of two Lamiaceae species (*Thymbra capitata* and *Thymus sipyleus subsp. rosulans*): in vitro, in silico and ex vivo approaches. Molecules 27:9029

Ma Y, Sharkey M, Coggins AM, Stubbings W, Gealy MG, Harrad S (2025) Concentrations of perfluoroalkyl substances in sediments and wastewater treatment plant-derived biosolids from Ireland. Sci Total Environ 979:179380

Matin TAB, Ghasemi N, Ghodrati K, Ramezani M (2018) Synthesis and characterization of silver nanoparticles using *Thymbra spicata* L. herbal extract for removing methylene blue dye from aqueous solutions. Bulgarian Chem Commun 50:345–358

Mbarki F, Selmi T, Kesraoui A, Seffen M, Gadonneix P, Celzard A, Fierro V (2019) Hydrothermal pre-treatment, an efficient tool to improve activated carbon performances. Ind Crops Prod 140:111717

Melnyk IV, Tomina VV, Stolyarchuk NV, Seisenbaeva GA, Kessler VG (2021) Organic dyes (acid red, fluorescein, methylene blue) and copper (II) adsorption on amino silica spherical particles with tailored surface hydrophobicity and porosity. J Mol Liq 336:116301

Mobarak M, Selim AQ, Mohamed EA, Seliem MK (2018) A superior adsorbent of CTAB/H_2O_2 solution–modified organic carbon rich-clay for hexavalent chromium and methyl orange uptake from solutions. J Mol Liq 259:384–397

Mobarak M, Mohamed EA, Selim AQ, Eissa MF, Seliem MK (2019) Experimental results and theoretical statistical modeling of malachite green adsorption onto MCM–41 silica/rice husk composite modified by beta radiation. J Mol Liq 273:68–82

Moheb M, El-Wakil AM, Awad FS (2025) Highly porous activated carbon derived from the papaya plant (stems and leaves) for superior adsorption of alizarin red s and methylene blue dyes from wastewater. RSC Adv 15:674–687

Moralı U, Demiral H, Şensöz S (2018) Optimization of activated carbon production from sunflower seed extracted meal: Taguchi design of experiment approach and analysis of variance. J Clean Prod 189:602–611

Nguyen DLT, Binh QA, Nguyen XC, Nguyen TTH, Vo QN, Nguyen TD, Tran TCP, Nguyen TAH, Kim SY, Nguyen TP, Bae J, Kim IT, Le QV (2021) Metal salt-modified biochars derived from agro-waste for effective congo red dye removal. Environ Res 200:111492

Okolie JA, Nanda S, Dalai AK, Kozinski JA (2021) Optimization studies for hydrothermal gasification of partially burnt wood from forest fires for hydrogen-rich syngas production using Taguchi experimental design. Environ Pollut 283:117040

Oladipo AA, Gazi M (2015) Two-stage batch sorber design and optimization of biosorption conditions by Taguchi methodology for the removal of acid red 25 onto magnetic biomass. Korean J Chem Eng 32:1864–1878

Omi FR, Rastgar M, Mohseni M, Singh U, Dilokekunakul W, Keller R, Wishart D, Wessling M, Vecitis CD, Sadrzadeh M (2025) Removal of emerging contaminants from water using novel electroconductive membranes in a hybrid membrane distillation and electro-Fenton process. Sep Purif Technol 357:130083

Ozcan MM, Ozkan G (2018) The total phenol, flavonol amounts, antioxidant capacity and antiradical activity of some thyme species growing in Turkey. J Chil Chem Soc 63:4051–4056

Pandey S, Do JY, Kim J, Kang M (2020) Fast and highly efficient removal of dye from aqueous solution using natural locust bean gum based hydrogels as adsorbent. Int J Biol Macromol 143:60–75

Patra BR, Nanda S, Dalai AK, Meda V (2021) Taguchi-based process optimization for activation of agro-food waste biochar and performance test for dye adsorption. Chemosphere 285:131531

Peksel A, Arisan-Atac I, Yanardag R (2010) Evaluation of antioxidant and antiacetylcholinesterase activities of the extracts of *Pistacia atlantica* desf. leaves. J Food Biochem. https://doi.org/10.1111/j.1745-4514.2009.00290.x

Prieto P, Pineda M, Aguilar M (1999) Spectrophotometric quantitation of antioxidant capacity through the formation of a phosphomolybdenum complex: specific application to the determination of vitamin E. Anal Biochem 269:337–341

Rafaqat S, Ali N, Torres C, Rittmann B (2022) Recent progress in treatment of dyes wastewater using microbial-electro-Fenton technology. RSC Adv 12:17104–17137

Rasheed T (2022) Magnetic nanomaterials: greener and sustainable alternatives for the adsorption of hazardous environmental contaminants. J Clean Prod 362:132338

Rehman MSU, Kim I, Han J-I (2012) Adsorption of methylene blue dye from aqueous solution by sugar extracted spent rice biomass. Carbohydr Polym 90:1314–1322

Rose PK, Poonia V, Kumar R, Kataria N, Sharma P, Lamba J, Bhattacharya P (2023) Congo red dye removal using modified banana leaves: adsorption equilibrium, kinetics, and reusability analysis. Groundw Sustain Develop 23:101005

Sen TK (2023) Adsorptive removal of dye (methylene blue) organic pollutant from water by pine tree leaf biomass adsorbent. Processes 11:1877

Sen TK, Afroze S, Ang HM (2011) Equilibrium, kinetics and mechanism of removal of methylene blue from aqueous solution by adsorption onto pine cone biomass of *Pinus radiata*. Water Air Soil Pollut 218:499–515

Shukla AK, Alam J, Mallik S, Ruokolainen J, Kesari KK, Alhoshan M (2024) Optimization and prediction of dye adsorption utilising cross-linked chitosan-activated charcoal: response surface methodology and machine learning. J Mol Liq 411:125745

Singleton VL, Orthofer R, Lamuela-Raventós RM (1999) [14] Analysis of total phenols and other oxidation substrates and antioxidants by means of folin-ciocalteu reagent. Methods in Enzymology. Elsevier, pp 152–178

Sismanoglu S, Akalin MK, Akalin GO, Topak F (2023) Effective removal of cationic dyes from aqueous solutions by using black cumin (*Nigella sativa*) seed pulp and biochar. BioRes 18:3414–3439

Sismanoglu S, Abdulmahdi Shakir S, Sahin Kol H, Hani YB, Aghlara E, Akalin MK (2025) Comparison of effective removal of cationic malachite green dye from waste water with three different adsorbents: date palm, date palm biochar and phosphated biochar. Int J Environ Anal Chem 105:981–1000

Soury R, Jabli M, Latif S, Alenezi KM, El Oudi M, Abdulaziz F, Teka S, El Moll H, Haque A (2022) Synthesis and characterization of

a new meso-tetrakis (2,4,6-trimethylphenyl) porphyrinto) zinc(II) supported sodium alginate gel beads for improved adsorption of methylene blue dye. Int J Biol Macromol 202:161–176

Tan YH, Abdullah MO, Nolasco-Hipolito C, Ahmad Zauzi NS (2017) Application of RSM and Taguchi methods for optimizing the transesterification of waste cooking oil catalyzed by solid ostrich and chicken-eggshell derived CaO. Renew Energy 114:437–447

Tohdee K, Semmad S, Jotisankasa A, Jongsomjit B, Somsiripan T, Asadullah (2024) Sustainable adsorption of methylene blue onto biochar-based adsorbents derived from oil palm empty fruit branch: performance and reusability analysis. Bioresour Technol Rep 25:101755

Uddin J, Abdur R, Hossain R, Aziz S, Jamal MS, Shaikh AA, Hossain M (2024) Phase tunable nickel doped Mn_3O_4 nanoparticle synthesis by chemical precipitation: kinetic study on dye degradation. Nanoscale Adv 6:902–909

Ullah N, Ali Z, Khan AS, Adalat B, Nasrullah A, Khan SB (2024) Preparation and dye adsorption properties of activated carbon/clay/sodium alginate composite hydrogel membranes. RSC Adv 14:211–221

Ullah N, Ali Z, Khan AS, Adalat B, Nasrullah A, Shaheen R (2025) Fabrication of activated carbon, polyvinyl alcohol–based alginate composite beads for the removal of methylene blue. Biomass Conv Bioref. https://doi.org/10.1007/s13399-025-06813-0

Vigneshwaran S, Sirajudheen P, Karthikeyan P, Meenakshi S (2021) Fabrication of sulfur-doped biochar derived from tapioca peel waste with superior adsorption performance for the removal of Malachite green and Rhodamine B dyes. Surf Interf 23:100920

Wu G, Zhou C, Li H, Xia S, Zhu Y, Han J, Xing W (2023) Controlled fabrication of the biomass cellulose aerogel@ZIF-8 nanocomposite as efficient and recyclable adsorbents for methylene blue removal. Ind Crops Prod 193:116169

Xia Y-F, Yuan H-Q, Qiao C, Li W, Wang R, Chen P, Li YX, Bao GM (2024) Multifunctional Eu^{3+}-MOF for simultaneous quantification of malachite green and leuco-malachite green and efficient adsorption of malachite green. J Hazard Mater 465:133386

Xiao W, Garba ZN, Sun S, Lawan I, Wang L, Lin M, Yuan Z (2020) Preparation and evaluation of an effective activated carbon from white sugar for the adsorption of rhodamine B dye. J Clean Prod 253:119989

Yusuff AS, Ajayi OA, Popoola LT (2021) Application of Taguchi design approach to parametric optimization of adsorption of crystal violet dye by activated carbon from poultry litter. Sci Afr 13:e00850

Zavala-Flores E, Flores-López Z, Alonso-Nuñez L, Espinoza-Gómez G H (2024) Removal and adsorption kinetics of methylene blue dye by pristine cotton husk bracts (*Gossypium hirsutum* L.) from agroindustrial waste. Ind Crops Prod 209:117947

Publisher's Note Springer Nature remains neutral with regard to jurisdictional claims in published maps and institutional affiliations.